

604985

FCI  
CHIEF, BUREAU OF SHIPS TECHNICAL LIBRARY

WELD CRACKING IN SUBMARINE STEELS

COPY 2 OF 3

by

HARD COPY \$.

MICROFICHE \$.

R. E. Travis and C. M. Adams, Jr.

FINAL REPORT OF AN INVESTIGATION CONDUCTED

by

Massachusetts Institute of Technology  
Division of Sponsored Research  
Cambridge 39, Massachusetts

In Cooperation With

Bureau of Ships, Code 634B  
U. S. Department of the Navy

Contract NObs 88370

Project Serial No. SR-007-01-01, Task 855

June, 1964

## TABLE OF CONTENTS

	<u>Page</u>
TITLE PAGE . . . . .	
TABLE OF CONTENTS . . . . .	
LIST OF TABLES . . . . .	
LIST OF FIGURES . . . . .	
I. INTRODUCTION . . . . .	1
II. APPARATUS . . . . .	2
III. THERMAL RELATIONSHIPS IN HINDERED CONTRACTION . . . . .	5
IV. EXPERIMENTAL CONDITIONS . . . . .	12
V. SPECIAL THERMAL STUDIES . . . . .	13
VI. EFFECT OF PROCESS VARIABLES ON REACTION LOADS AND CRACKING . . . . .	15
VII. CONCLUSIONS . . . . .	16
VIII. BIBLIOGRAPHY . . . . .	21
TABLES . . . . .	
FIGURES . . . . .	

## LIST OF TABLES

<u>Table No.</u>	<u>Title</u>
I	Chemical Composition of Plate and Filler Alloys
II	Welding Procedures
III	Mechanical Properties of Plate
IV	Assumed Values of Thermal Constants Used in Equations (3A), (6A), (7A), (8A), and (9A)
V	Correlation of Weld Metal Properties with Energy Input

## LIST OF FIGURES

<u>Figure No.</u>	<u>Title</u>
1.	Horizontal Lever Arm Apparatus Design
2.	Fixed End U-bar Design
3.	Pinned End U-bar Design
4.	Specimen Design for Pure Transverse Loading
5.	9 Inch Moment Arm Specimen Design
6.	Calculated and Measured Strain Gage Readings for U-bar Calibration
7.	Microstructure of Location Having 1300°F Peak Temperature in HY-80 Magnification: 100X Nitel Etch
8.	Microstructure of Location Having 1300°F Peak Temperature in HY-80 Magnification: 500X
9.	Dendrite Microstructure of Weld Metal in HY-80 Near Fusion Boundary
10.	Dendrite Spacing in HY-80 Weld Metal (Near Fusion Boundary) as a Function of Arc Energy Input
11.	Effect of Arc Energy Input on Separating Force
12.	Effect of Arc Energy Input on Separating Force
13.	Effect of Arc Energy Input on Separating Force
14.	Effect of Arc Energy Input on Cracking
15.	Effect of Bending Moment on Cracking
16.	Effect of Arc Energy Input on Separating Force
17.	Effect of Arc Energy Input and Number of Passes on Separating Force
18.	Effect of Arc Energy Input on Separating Force
19.	Effect of Arc Energy Input on Separating Force
20.	Effect of Arc Energy Input and Number of Passes on Separating Force

LIST OF FIGURES (Continued)

<u>Figure No.</u>	<u>Title</u>
21.	Effect of Arc Energy Input and Number of Passes on Bending Moment
22.	Effect of Plate Composition on Separating Force
23.	Effect of Plate Composition on Separating Force
24.	Effect of Welding Process (MIG or Submerged Arc) on Separating Force
25.	Effect of Postheat on Separating Force

## I. INTRODUCTION

The following report describes results of the first year's work on a research program directed to the behavior of submarine steels when welded under conditions of hindered thermal contraction.

The principal objectives of the investigation have been to make quantitative or semi-quantitative assessments of procedural and compositional factors in the development of residual stresses or cracking in or near welds cooling while subjected to external restraint, the external restraining apparatus being so instrumented<sup>1,2</sup> as to give continuous information on the magnitudes of bending moment and separating force to which the welds are subjected. It should be noted many of the interesting responses exhibited by materials in the HY-80 category occur long after the weld has cooled to ambient temperature; this report might well have been entitled "Delayed Mechanical Responses of Welds Subjected to Hindered Contraction". A further objective has been to refine and compare different types of instrumented restraining apparatus to the end of developing the most sensitive and meaningful tests possible for evaluating and comparing materials and procedures from the standpoints of how they influence stress buildup and cracking.

The principal variables which entered into the experimental program were: arc energy input, plate composition, filler metal composition, the presence or absence of a bending moment in the geometry of the restraint, the initial heat treatment of the plate, multi-pass welding procedures, and welding process (MIG or submerged arc). In addition, there was some study

of the effects of immediate post weld heat treatment. Also, plate thickness may be listed as a variable, since more than one thickness was involved.

In addition to making essentially mechanical observations of contraction forces, enough thermal data on weld cooling rates and peak temperature distributions were collected to establish the heat flow conditions associated with all experimental welds. The investigation also included metallographic study of weld metal and the immediate weld heat affected zone, but correlations with mechanical behavior have, to date, proven negative.

## II. APPARATUS

Three different sets of apparatus have been used to study hindered contraction under different geometries and magnitudes of restraint; a horizontal lever arm shown in Figure 1, a fixed end U-bar shown in Figure 2, and a pinned end U-bar shown in Figure 3. Of the three apparatus the horizontal lever arm has the lowest overall stiffness. Through the use and location of pivot pins, it is possible with the horizontal lever arm to impose any desired ratio of transverse bending moment to separating force on the specimen weld, and it is also possible to restrain welds in the absence of a transverse bending moment. A movable fulcrum on the horizontal lever arm permits a wide degree of adjustability in the elastic stiffness of the restraining system.

The fixed end U-bar accords moderately high restraints, and has the virtue of no mechanical linkages between the test weld and the stress measuring part of the system. However, the ratio of transverse bending moment to separating force is a nonadjustable feature of the fixed end

U-bar. The U-bar is an outgrowth of the keyhole plate used in earlier studies<sup>1</sup>, which was in turn a modification of the NRL slotted plate crack susceptibility test specimen; the U-bar has several signal advantages over the keyhole plate, including far more precise analytical interpretation of results, the possibility of using preheat, lower machining cost per specimen, and amenability to the use of run-on and run-off tabs.

The pinned end U-bar affords the advantage of restraining the test weld in the absence of a bending moment; however, the elastic stiffness of the system is fixed.

The types of test specimens used on the horizontal lever arm and pinned end U-bar are shown in Figures 4 and 5, one of which (Figure 5) causes a bending moment as well as a separating force to be imposed upon the weld. The weld specimen used on the fixed end U-bar is shown as mounted in Figure 2. In the horizontal lever arm apparatus and pinned end U-bar, the specimen plates are affixed to the ends of the arms by means of hardened steel pivot pins of 0.5 inch diameter, an arrangement which renders the bending moment imposed on the weld fully determinant. On the fixed end U-bar, the specimen plates must be welded into position for each run; after completion of the test, the specimens are flame cut from the U-bar which can be calibrated and used for a large number of runs. Welded connections have been used to minimize backlash in mechanical joints; on the fixed end U-bar apparatus, the auxiliary structural welds are located and dimensioned so that there is no hazard of yielding or cracking in any but the test weld location.

All three sets of restraining apparatus were calibrated on a tensile testing machine. An analysis of the U-bar as a curved beam<sup>3</sup>, checked by calibration, (Figure 6) has led to the following equations for separating force, F, and bending moment, M, acting at the location where the straight and curved sections are tangent:

$$F = \frac{0.2065S_1 - 0.562S_0}{0.2398} \quad \dots \dots \dots (1)$$

$$M = \frac{2.72S_0 - 0.96S_1}{0.2398} \quad \dots \dots \dots (2)$$

where

$S_1$  = the absolute magnitude of the compressive stress measured at the inside strain gage location, psi.

$S_0$  = the absolute magnitude of the tensile stress measured at the outside strain gage location, psi.

Using these equations, the applied bending moment and separating force at any instant during or after welding can immediately be determined from pertinent strain gage readings. With the U-bar apparatus, the relationship between separating force and bending moment, as reflected in Equations (1) and (2), is essentially more complicated than with the horizontal lever machine. With the horizontal lever machine, if the specimen is designed to produce a bending moment, its magnitude is simply the separating force times the moment arm.

In this investigation, most of the work was done using the fixed end and the pinned end U-bar, because this imposes the severest restraint;

even so, it was only possible to induce cracking using rather extreme welding procedures. The lever arm apparatus was only used to study the effects of post-heat, for which it is ideally suited. The pinned end U-bar was used in this investigation only when it was desired that no bending moment be imposed on the weld by external restraint; accordingly, only the specimen design shown in Figure 4 was used with the pinned end U-bar.

In the graphical presentation of data, only the separating force is plotted as a function of time after completion of the weld. Graphs showing the bending moment (imposed by the fixed end U-bar) have not provided any useful additional information, and so are not presented in this report. So far, the only thing which seems significant is whether or not a large bending moment is present as part of the restraint, because only in the presence of a bending moment is cracking ever observed.

### III. THERMAL RELATIONSHIPS IN HINDERED CONTRACTION

The cooling of a weld under hindered contraction must be considered from two distinctly different points of view. The rate with which the weld and immediate heat-affected zone cool, establishes how rapidly the weld can become strong enough to sustain an elastic load. In addition, the weld cooling rate influences metallurgical structure and strength and thereby the maximum load which the weld can be expected to sustain elastically at room temperature. The centerline cooling rate depends primarily upon conduction of the heat into the surrounding cold metal plate, and is little influenced by convection or radiation heat transfer from the plate to the air. On the other hand, the

overall rate with which the entire specimen loses heat to the surroundings establishes the rate of total solid contraction on the part of the plate being welded, and is therefore an essential part of the loading mechanism involved. This overall loss of heat from the plate takes place primarily by convection and radiation to the surroundings. (Redistribution of heat within the plate does not effect important dimensional changes; it is mainly the heat that escapes entirely from the plate which is reflected in gross solid contraction.)

These concomitant and related cooling rates may, in a sense, be regarded as competitive. For example, if the centerline cooling rate were large and the overall rate of heat loss quite small, the hottest part of the weld would acquire strength before most of the load was applied, plastic strain would be minimized, and shrinkage distortion effects quite large. If, on the other hand, the centerline cooling rate is low, as with high preheat, and solid contraction effects make themselves felt while the weld metal is still very hot, substantial plastic flow obtains, and net shrinkage is relatively low. Thus, thermo-mechanical effects depend fundamentally upon the rate of overall cooling as compared to the rate of centerline cooling in the subject weld.

It is possible to make a direct mathematical comparison between the centerline cooling rate of the weld and the overall rate of heat transmission to the surroundings. There is one special case which can be analyzed quite simply to show the effects of weld variables on these two different cooling rates. Consider the instant at which the weld metal has just become completely solid; the weld centerline is cooling at a rate which, for the conditions of this investigation, is accurately expressed by<sup>4</sup>:

$$\frac{dT}{d\theta} = 2 \pi K \rho C_p \left( \frac{Vt}{q} \right)^2 (T_m - T_o)^3 \dots \dots \dots (3)$$

where

- K = thermal conductivity of the metal
- $\rho$  = density of the metal
- $C_p$  = specific heat of the metal
- V = velocity of arc travel
- t = thickness of plate
- q = arc power
- $T_m$  = melting point of the metal
- $T_o$  = the initial temperature of the metal
- $\frac{dT}{d\theta}$  = centerline cooling rate

Using reasonable values for the thermal properties of steel, a dimensional equation giving the cooling rate in  $^{\circ}\text{F}/\text{sec}$  is:

$$\frac{dT}{d\theta} = 120 \frac{Vt}{q}^2 (T - T_o)^3 \dots \dots \dots (3A)$$

where  $q/V$  is in Joules/inch, the plate thickness,  $t$ , in inches, and temperatures in  $^{\circ}\text{F}$ .

The transverse shrinkage experienced by the weld depends on the thermal coefficient of solid contraction,  $\alpha$ , and the coefficient of heat transfer,  $h$ , from the surface of the cooling weldment to the surroundings, in addition to the other thermal variables identified above. The kinetics of transverse shrinkage can be expressed in either of two ways. Equation (4), below,

gives the net transverse shrinkage,  $W$ , and Equation (5) the rate of shrinkage,  $\frac{dW}{d\theta}$ , as a function of time,  $\theta$ , after completion of the weld. Strictly speaking, these equations pertain to a relatively short weld, in which longitudinal shrinkage has little effect, and which is free to undergo lateral thermal contraction; there is no external restraint.

$$W = \frac{q}{V} \frac{\alpha}{\rho C_p t} \left( 1 - e^{-\frac{2 h \theta}{\rho C_p t}} \right) \dots (4)$$

$$\frac{dW}{d\theta} = \frac{q}{V} \frac{2 h \alpha}{\rho C_p t^2} e^{-\frac{2 h \theta}{\rho C_p t}} \dots (5)$$

The exponential form of Equation (5) properly suggests that the rate of shrinkage is the greatest immediately after completion of the weld. Of course, the total shrinkage reaches its maximum value long after completion of the weld, when the metal has cooled to ambient temperature. Equations (6) and (7) show the values at these extremes. Equation (6) gives the maximum total transverse shrinkage and Equation (7) gives the maximum (initial) rate of shrinkage experienced by the weld.

$$W = \left( \frac{q}{V} \right) \frac{\alpha}{\rho C_p t} \dots (6)$$

(when  $\theta$  is large)

$$\frac{dW}{d\theta} = \left( \frac{q}{V} \right) \frac{2 h \alpha}{(\rho C_p t)^2} \dots (7)$$

(when  $\theta$  is zero)

Expressing these in dimensional form:

$$W = \frac{(q/vt)}{5,400,000} \quad (\text{inches}) \quad \dots \dots \dots (6A)$$

$$\frac{dW}{dt} = \frac{(q/vt^2)}{1,500,000} \quad (\text{inch/hr}) \quad \dots \dots \dots (7A)$$

where, again, are energy input is in Joules/inch, and plate thickness in inches.

If, instead of being free to contract, the plates are completely restrained, it is possible to express the average transverse stress developed in the weld. Equation (8) gives the maximum transverse stress which could possibly be developed in a restrained weld. The overall transverse width of the weldment, W, might also be regarded as the separating between the clamps of a perfectly immovable restraining fixture. The maximum stress would only be realized if all the thermal strain were elastic. The symbol, t', refers to the depth of the minimum load-carrying section in the weld, which in general will be smaller than t, the plate thickness. These equations pertain only to the first of several passes used in producing a joint.

$$S = \left( \frac{q}{v} \right) \frac{\alpha E}{\rho C_p t' W} \quad \dots \dots \dots (8)$$

where

S = transverse stress in the weld metal

E = modulus of elasticity

Expressing Equation (8) dimensionally:

$$S = 6 \frac{q}{V t' W} \dots\dots\dots (8A)$$

The rate of stress buildup in the weld,  $\frac{dS}{dq}$ , is in some ways even more interesting than the total maximum stress which can be developed, and this is given by:

$$\frac{dS}{dq} = \left(-\frac{q}{V}\right) \frac{2 h \alpha E}{(\rho C_p)^2 t t'} \dots\dots\dots (9)$$

Expressing Equation (9) dimensionally:

$$\frac{dS}{dq} = 0.3 \frac{q}{V t t' W} \dots\dots\dots (9A)$$

where

S is in lbs/inch<sup>2</sup> min.

In Equations (3A), (6A), (7A), (8A), and (9A) the numerical values which can be used to evaluate the constants are listed in Table V.

The load carrying section of the weld, represented by t', can be measured or estimated from the weld arc energy input using the following approximate relationships:

$$t' = \frac{1}{500} \frac{q}{\sqrt{\quad}} \quad (60^\circ \text{ included angle, first pass}) \dots\dots\dots (10)$$

$$t' = \frac{1}{300} \frac{q}{\sqrt{\quad}} \quad (30^\circ \text{ included angle, first pass}) \dots\dots\dots (11)$$

The main purpose in presenting these mathematical expressions is to show that the operating variables which influence both the centerline cooling rate and the overall shrinkage rate have generally opposite effects. Thus a high arc energy input tends to reduce the centerline cooling rate but increases the rate of transverse shrinkage. Decreasing the plate thickness exerts the same two effects.

The effect of pre-heat is somewhat more complicated. If both the restraining fixture and the weldment are uniformly pre-heated to some elevated temperature, there will be shrinkage of both the weldment and of the restraining fixture, since both are losing heat to the environment. There will still be stresses developed in the weld, because it has excess heat to lose to the surroundings. Since the effect of pre-heat is to reduce the centerline cooling rate of the weld (Equation (1)), the effect will be to favor plastic deformation of the weld and thereby reduce stress or distortion. If, on the other hand, only the weld is pre-heated and the restraining fixture remains of fixed dimensions, pre-heat contributes to the total thermal contraction load the weldment imposes upon itself, and the effect can be to increase the stress or distortion resulting from welding.

Thus all of the important thermal variables of welding have opposing influences on shrinkage rate and centerline cooling rate. Finally, it should be noted that environmental conditions influence the magnitude of  $h$ , the surface coefficient of heat transfer, which has a direct bearing on the transverse shrinkage rate but no important effect on the centerline cooling rate. For example, under the same conditions of arc energy input, plate thickness, and pre-heat, the submerged arc process differs from the MIG process in that surface heat transfer and therefore transverse shrinkage is less with the submerged arc because of the insulating character of the slag covering.

Because of this, the two processes exhibit different rates and magnitudes of self-imposed loading under conditions of hindered contraction.

#### IV. EXPERIMENTAL CONDITIONS

The results reported herein pertain mostly to single pass arc welds deposited in 1/2 inch, and 1 inch HY-80 steel plates using MIG and submerged arc welding procedures. Three different heats of HY-80 were used, having slightly differing chemistries, hardenability, and (presumably) susceptibility to weld cracking. Two different filler wires were used. Plate and filler compositions are presented in Table I. All welding was fully automatic and the summary of welding conditions is presented in Table II. The combinations of voltage, amperage, wire diameter, and series inductance which were used with the MIG process resulted in a relatively short arc length with fairly insensitive response, a set of circumstances which was found to produce the most regular penetration and weld bead contour. The conditions actually approached without quite reaching short circuiting arc operation. Two joint geometries were used: 60° included angle, single Vee, 1/16 inch root opening, for the 1/2 inch plate; 30° included angle, double Vee, 1/16 inch root opening, for the 1 inch plate.

Heats A and X were received in the heat treated condition while heat P was received as hot rolled plate. The hot rolled plate was austenitized at 1650°F for one hour, water quenched, tempered at 1275°F for one hour, and water quenched. The mechanical properties of the plates are shown in Table III.

## V. SPECIAL THERMAL STUDIES

During several of the cracking experiments, peak temperatures and critical cooling rates experienced during welding were established using experimental techniques previously developed.<sup>5,6</sup>

Temperature measurements were made by means of platinum-platinum 10% rhodium thermocouples, percussively welded to surface locations. Surface temperature measurements made by percussive weld thermocouples are in error by amounts which depend on the diameters of the thermocouple wires, if the thermocouple is larger than 0.020 inch diameter. Using thermocouple wires heavier than this results in low readings because of conduction losses along the thermocouple leads. With wire diameters smaller than 0.020 inch, temperature measurements are independent of wire diameter, and are presumed correct. In this investigation, thermocouple leads were 0.005 inch in diameter, and the leads were independently welded to the plate surface location of interest, such that the thermocouple bead was in fact composed of steel residing in the plate surface.

Surface temperature measurements have been correlated with observations of macrostructure and microstructure. Determinations were made of the peak temperature associated with the outermost etching boundary in HY-80, which was definitely established as  $1300 \pm 30^\circ\text{F}$ . This observation prevailed for welds embracing a ten-fold range of cooling rates. With this piece of information, welds in HY-80 can be thermally "diagnosed" by measuring the extent of the heat-affected zone.

The macrostructure associated with this  $1300^\circ\text{F}$  peak temperature experienced is shown in Figures 7 and 8, for HY-80 at 100 and 500

magnifications. The transition zone is associated with the lower critical, and consists of a dispersion of martensite or very fine pearlite (depending on the cooling rate) in a matrix of substantially unaltered base material.

Correlations of weld metal structure with arc energy input for many alloys (other than steel) have shown that dendrite arm spacing is inversely proportional to the square root of arc energy input. Attempts to perform this type of correlation of dendrite structures in HY-80 have met with the difficulty that solid state transformations generally obscure dendrite patterns. However, under certain conditions dendrite patterns such as that shown in Figure 9 can be resolved at locations near the fusion boundary, which is the area of most interest with respect to delayed cold cracking. For some reason the dendrite pattern near the center of the weld is completely obscured by a Widmanstätten type transformation, the coarseness of which also varies directly with arc energy input (inversely with solidification rate). The way in which the dendrite spacing varies with arc energy input near the fusion boundary is shown in Figure 10; this linear correlation conforms with that earlier observed with aluminum-, copper-, and nickel-rich alloys.<sup>7,8</sup> An understanding of these relationships and the ability to measure the dendrite spacing at the fusion boundary may lead, through further study, to establishment of relationships among dendrite spacing, dimensions of the heat-affected zone, arc energy input, and delayed cracking of welds subjected to hindered contraction.

## VI. EFFECT OF PROCESS VARIABLES ON REACTION LOADS AND CRACKING

The data on the development of transverse reaction loads and moments and the incidence of cracking for all conditions studied in this investigation, are summarized graphically in Figures 11 through 25. All the curves are transcribed and calculated from continuous strip chart records of strain gage output.

In reading the curves of separating force or bending moment vs. time, the following ground rules are important:

(1) Unless otherwise designated, all determinations are for single-pass welds, which are so deposited as to represent the first pass in a multi-pass welding procedure. In these cases, the weld deposit is substantially smaller in load carrying section than the surrounding plate.

(2) The convention used throughout is that positive separating force reflects net tension transverse to the weld. A negative separating force implies compression.

(3) The apparatus was sensitive enough to determine irregularities in the development of transverse loads and bending moments. Since these irregularities are themselves of some interest, the curves have been drawn as faithful representatives of the original data with any "wiggles" left in. Both yielding and cracking are phenomena which tend to take place discontinuously.

(4) Over the course of the investigation it was learned that the strain recorders gave very delicate indications of cracking. Cracking always initiated at the end of the weld nearest the restraining fixture.

Cracking was never detected metallographically in any specimen in which it was not also detected by the strain recorder. Cracking is indicated on the curves by small arrows labeled "crack observed", which indicate the instant at which cracking was first observed either on the strain recorder or optically. Usually the two observations coincided.

(5) In all but one case the coordinates of the graphs are separating force and time after finish of welding. The one exception (Figure 21) shows the bending moment, acting at the center of the weld, as a function of time after finish of welding.

#### VII. CONCLUSIONS

(1) With these steels and filler materials, higher arc energy input per pass is generally associated with higher separating force. This is almost always true of the maximum separating force experienced, and, with few exceptions, is also true of the final steady separating force, (Figures 11, 12, 16 and 19). This relationship between separating force and arc energy input is generally true of the plain carbon or relatively low strength hardenable steels, whatever the welding process. With higher carbon hardenable compositions, the reverse is sometimes observed, because for these materials the effect of cooling rate may overwhelm the effect of the size of the weld deposit.

(2) With low energy single pass welds, the separating force may actually be negative (compressive), particularly when the weld is deposited under conditions of restraint which do not impose a bending moment (pinned end U-bar). This is interpreted to mean that plastic

deformation precedes the expansion effects associated with transformation of austenite (Figures 12 and 13).

(3) Low energy single pass submerged arc welds exhibit a remarkable reduction in separating force at times long after completion of welding (Figures 18, 19, 22 and 24). This effect was observed for all three plate compositions. All submerged arc welding in this program was done with filler A, so it has not yet been established whether this is characteristic of the filler, the process, or the combination. However, this very delayed reduction in separating force was not observed with the MIG process using either filler.

(4) As has been observed with other hardenable steels, cracking is generally favored by extremely low arc energy input, and the lower the arc energy input, the less the time delay associated with cracking (Figures 14 and 15). Under conditions of automatic welding, using run-on and run-off tabs so that no craters were present within the stress field, it was found exceedingly difficult to induce cracking with the filler and plate compositions used in this investigation. Furthermore, cracking was never rapid or catastrophic enough to be audible or to reflect major abrupt changes in observed reaction loads. Separating force continues to increase after the initiation of cracking. Observations of cracking were limited to Heat P. It was not found possible, even with extremely low arc energy inputs, to induce cracking in either Heat A or Heat X.

(5) The effects of variations in multi-pass welding procedures were as expected. Increasing the arc energy input per pass generally results in higher separating forces, and increasing the time delay between passes also increases separating forces. This also parallels earlier observations made with other hardenable steels.<sup>2</sup> During the actual deposition of a weld pass, there is some relief of reaction loads imposed by earlier passes, because of momentary expansion and stress relief accomplished by the arc heat, but there is a cumulative effect in that each weld pass adds to the final total reduction load.

(6) The delayed reduction in separating force, which seems peculiarly associated with the submerged arc process, has not been observed with high energy single pass deposits, but is marked with high energy multi-pass deposits (Figure 20). The effect is by no means small; Figure 20 shows a reduction in separating force the order of 13 tons acting on a load-carrying cross section of weld metal which was slightly greater than one square inch.

(7) Generally, the shape of the bending moment vs. time curve closely parallels the corresponding graph of separating force, for which reason the bending moment curves have not been included in this report. However, there are interesting effects on the bending moment noted with multi-pass procedures as shown in Figure 21. During actual deposition of a weld pass (other than the first) there is usually a fairly abrupt decrease in separating force (Figure 20) especially with high energy passes, and a simultaneous momentary increase in bending moment (Figure 21). This reflects the momentary non-uniform heat distribution and local perturbation of thermal strain which is developed during welding, and which quickly dissipates when

the heat supply ceases.

(8) Plate composition has a fairly small effect on separating force (Figure 22). As expected, at low energy input, the more hardenable plate gives a higher separating force, but with higher energy input, there is no significant difference (Figures 22 and 23). There is even a variation of plate thickness reflected in Figure 23; Heat A was 1 inch thick and Heats P and X were 1/2 inch thick.

(9) Immediate local application of post-heat delayed the development of separating force but does not reduce its magnitude (Figure 25). In fact separating force is increased. This is in sharp contrast to the behavior of higher carbon hardenable steels.<sup>2</sup>

(10) Although more data are needed to bring about a close correlation of thermal and mechanical events, examination of the graphs in the light of calculations made using Equations (3A), (8A), and (9A), conclusively indicate that weld metal deposited under conditions of restraint experiences some plastic deformation immediately after the supply of arc heat ceases. Usually there is a transition from plastic to elastic behavior during cooling and the residual transverse average stress is somewhat less than yield point magnitude, but seldom less than 1/4 the yield stress.

(11) The discontinuities reflected in many of the graphs are real and reflect irregular dimensional changes in or near the weld, many of which take place long after the weld has completely cooled to room temperature. These delayed effects bear on the magnitude of and time dependent changes

in residual stresses, and therefore have an importance which is somewhat separate from the question of weld cracking.

(12) The initial condition of heat treatment of an HY-80 composition evidently has very little to do with separating force or cold cracking. Heat A, which was heat treated to 159,500 psi yield, behaved quite like Heat P and X in most respects.

(13) Weld metal strength increases with decreasing arc energy input (Table V). Increased solidification and solid state cooling rates are considered responsible. It is important to note relatively high strength deposits, made by multipass low energy submerged arc, develop lower (maximum) separating forces than do lower strength high energy multipass deposits.

(14) Of the various restraining apparatus which have been used over the past 8 years in this laboratory, for medium strength hardenable steels the fixed end U-bar appears superior by reason of high sensitivity, reproducibility and convenience. Also, the circumstance of loading with the fixed end U-bar more nearly approximates that encountered in practice than is the case with any of the devices involving pinned connections.

VIII. BIBLIOGRAPHY

1. White, S. S., Moffatt, W. G., Adams, C. M., Jr., "Dynamic Measurement of Stress Associated with Weld Cracking," Welding Journal, Vol. 23, No. 4, April 1958.
2. Travis, R. E., Barry, J. M., Robinson, J. V., Moffatt, W. G., and C. M. Adams, Jr., "Fundamentals of Weld Behavior Under Hindered Contraction," The Welding Journal, 40, (2), Research Supplement, 49s-57s, (1961).
3. Den Hartog, J. P., "Advanced Strength of Materials," McGraw-Hill Book Company, Inc., 1952.
4. Adams, C. M., Jr., "Cooling Rates and Peak Temperatures in Fusion Welding," Welding Journal, Vol. 37, pg. 210s-215s, 1958.
5. Barry, J. M., Paley, Z., and Adams, C. M., Jr., "Heat Conduction from Moving Arcs in Welding," The Welding Journal, 42 (3), Research Supplement, 97s-104s (1963).
6. Paley, Z., Lynch, J. N., and Adams, C. M., Jr., "Heat Flow in Welding Heavy Steel Plate," The Welding Journal, 43 (2), Research Supplement, 71s-80s (1964).
7. Brown, P. E., and Adams, C. M., Jr., "Fusion-Zone Structures and Properties in Aluminum Alloys," The Welding Journal, 39 (12), Research Supplement, 520s-524s (1960).
8. Brown, P. E., and Adams, C. M., Jr., "Rapidly Solidified Alloy Structures," A.F.S. TRANS., Vol. 69, pp. 879-891 (1961).

TABLE I

Chemical Composition of Plate and Filler Alloys

<u>Plate</u>	<u>Thickness</u>	<u>C</u>	<u>Mn</u>	<u>Si</u>	<u>S</u>	<u>P</u>	<u>Mo</u>	<u>Ni</u>	<u>Cr</u>
A	1.0"	0.19	--	--	0.013	-	--	--	--
X*	0.5"	0.15	0.29	0.25	0.008	0.009	0.51	2.97	1.60
P**	0.5"	0.18	0.27	0.20	0.013	0.017	0.42	3.01	1.76
<u>Filler</u>	<u>Diameter</u>								
103	3/32"	0.054	1.50	0.61	0.006	0.005	0.31	1.00	0.02
A632	1/16"	0.042	1.31	0.50	0.013	0.007	0.46	1.36	0.10

\* Electric-furnace heat

\*\* Open-hearth heat

TABLE II

Welding Procedures

	<u>MIG</u>	<u>MIG</u>	<u>Submerged Arc</u>
Voltage (volts)	25	21	30
Amperage (amperes)	340	280	360-440
Travel Speed (ipm)	8-36	8-34	11-44
Plate Thickness (inch)	1/2, 1	1/2	1/2, 1
Filler Wire Feed Plate (ipm)	81	52	81
Filler Wire Diameter (inch)	3/32	1/16	3/32
Shielding	Argon-1% Oxygen	Argon-1% Oxygen	Flux
Shielding Gas Flow Rate (cfm)	40	40	--
Electrode Angle	Vertical	Vertical	15°
Inductance	Maximum	Maximum	--
Slope	Flat	Flat	--

TABLE III

Material	Orientation of Specimens	Mechanical Properties of Plates *		
		Yield Strength (0.2% offset) psi	Ultimate Tensile Strength psi	Elongation (%) 1" gage length
Heat F	perpendicular to weld	96,800	113,300	18.5
Heat P	parallel to weld	97,900	113,300	19.5
Heat X	perpendicular to weld	92,500	110,300	18.0
Heat X	parallel to weld	91,400	107,300	20.0
Heat A	parallel to weld	159,500	176,300	14.5

\* All values are an average of two test bars

TABLE IV

Assumed Values of Thermal  
Constants Used in Equations  
(3A), (6A), (7A), (8A) and (9A)

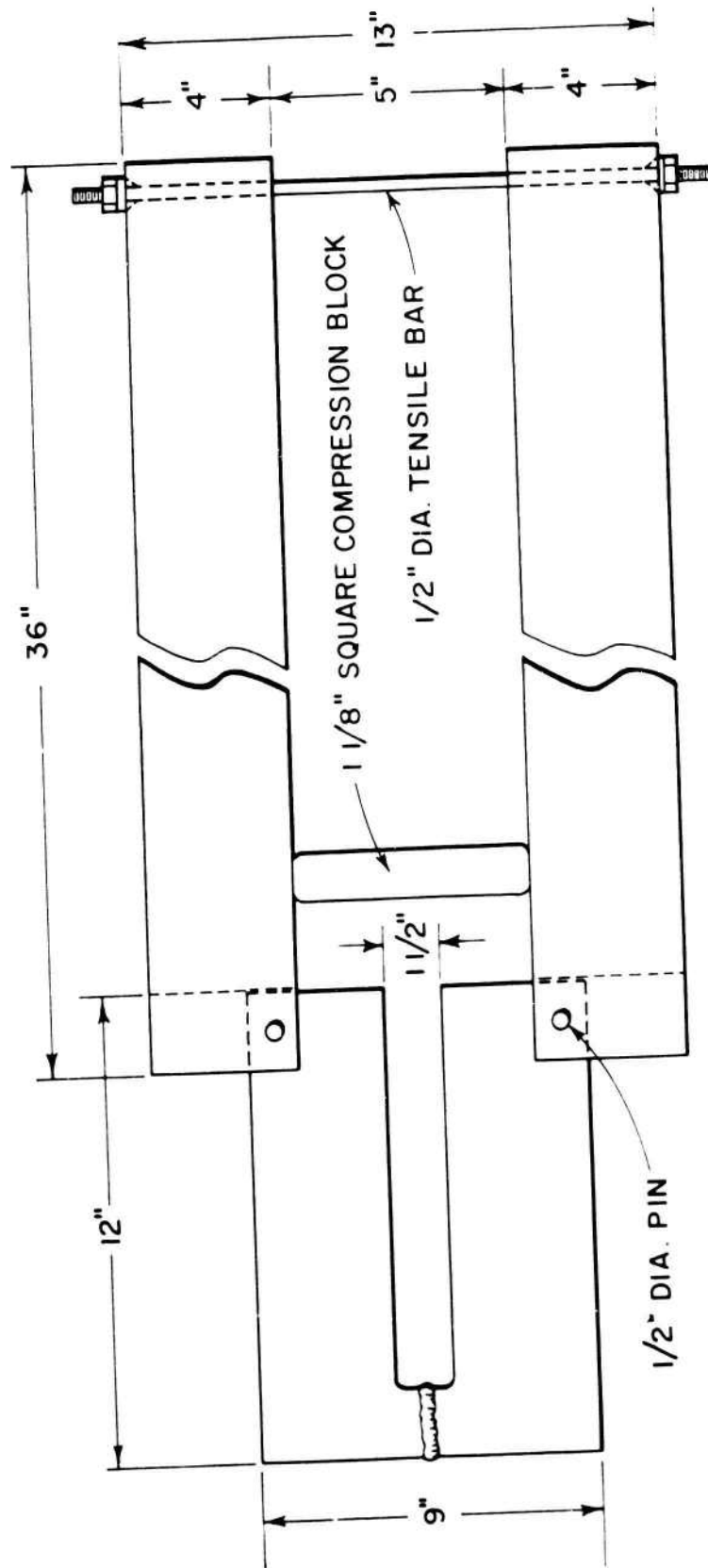
Coefficient of Expansion, $\alpha$ ,	$6.7 \times 10^{-6}$	$^{\circ}\text{F}^{-1}$
Density, $\rho$ ,	0.27	$\text{lb/in}^3$
Specific Heat, $C_p$ ,	0.14	$\text{BTU/lb } ^{\circ}\text{F}$
Heat Transfer Coefficient (average, steel to air, observed in welding, radiation + convection), $h$ ,	10	$\text{BTU/ft}^2 \text{ hr } ^{\circ}\text{F}$
Modulus of Elasticity, $E$ ,	$30 \times 10^6$	$\text{lb/in}^2$
Thermal Conductivity (average, observed in welding), $K$ ,	20	$\text{BTU/ft hr } ^{\circ}\text{F}$

TABLE V

Correlation of Weld Metal Properties with Energy Input

<u>Base Metal</u>	<u>Filler Metal</u>	<u>Energy Input (joules/inch)</u>	<u>Yield Strength, psi (0.2% offset)</u>	<u>Ultimate Tensile Strength, psi</u>	<u>Elongation (%) 1" gage length</u>
Heat P	B	68,300/pass 3 passes	--	119,000	--
Heat A	A	66,400/pass 3 passes	114,300	129,300	10.5
Heat A	A	66,400/pass 3 passes	107,300	124,000	12.5
Heat A	A	16,400/pass 8 passes	125,500	140,000	10.5
Heat A	A	17,400/pass 11 passes	129,500	144,000	10.5

All specimens were composed entirely of weld metal and taken parallel to welding direction.



NOTE: ARMS ARE 1 1/2" THICK.

Figure 1. Horizontal Lever Arm Apparatus Design

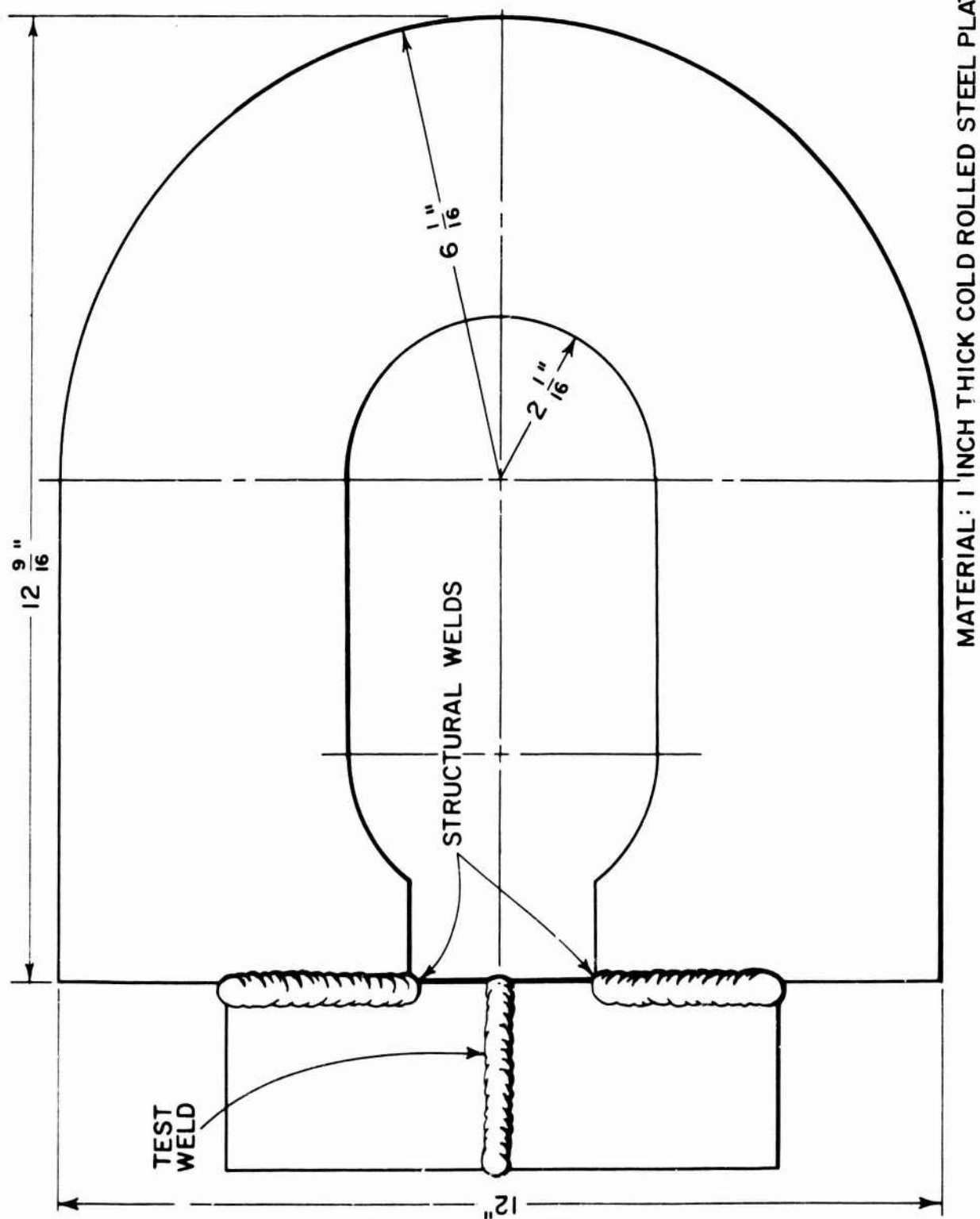
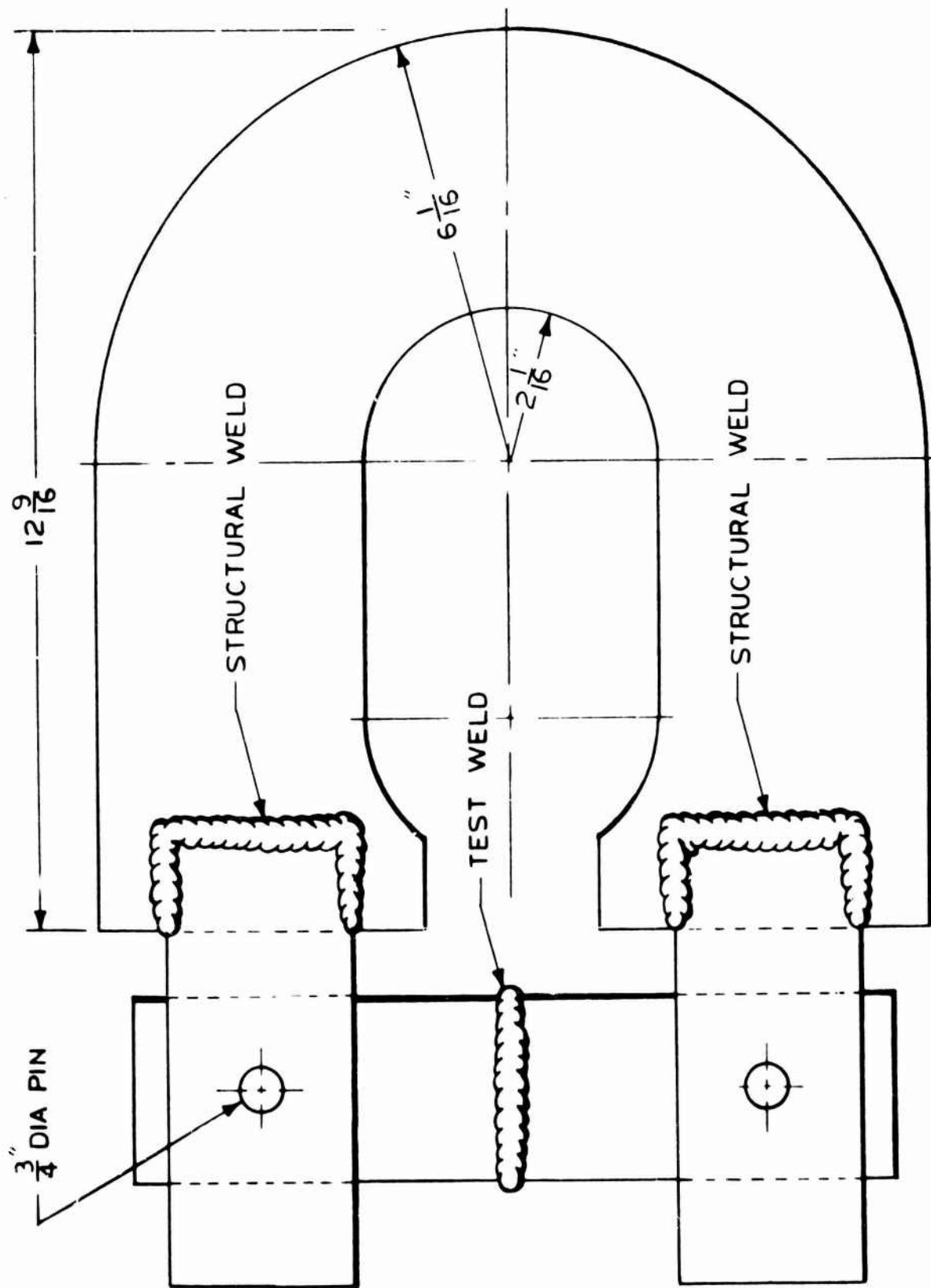


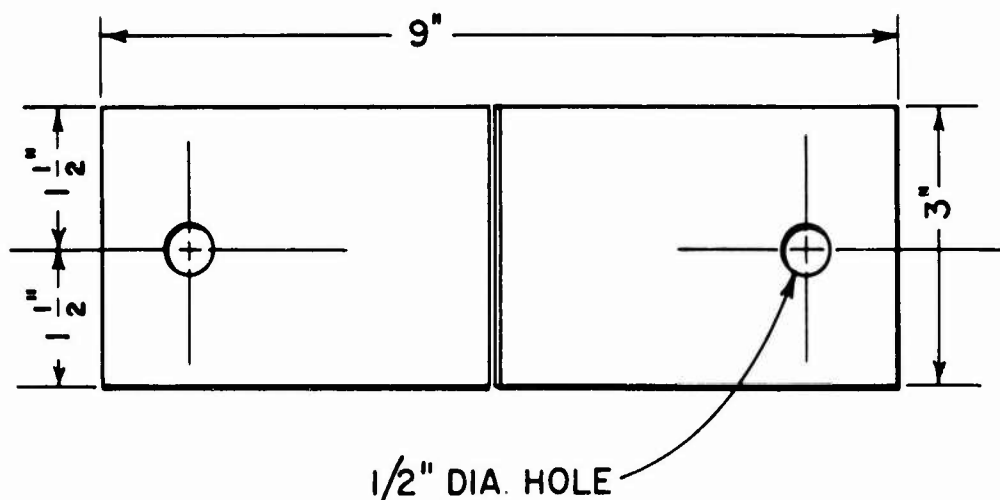
Figure 2.

Fixed End U-bar Design



MATERIAL: 1" COLD ROLLED STEEL PLATE

Figure 3. Pinned End U-bar Design



NOTE: PLATE IS 1/2" THICK.

Figure 4.

Specimen Design for Pure Transverse Loading  
with Horizontal Lever Arms

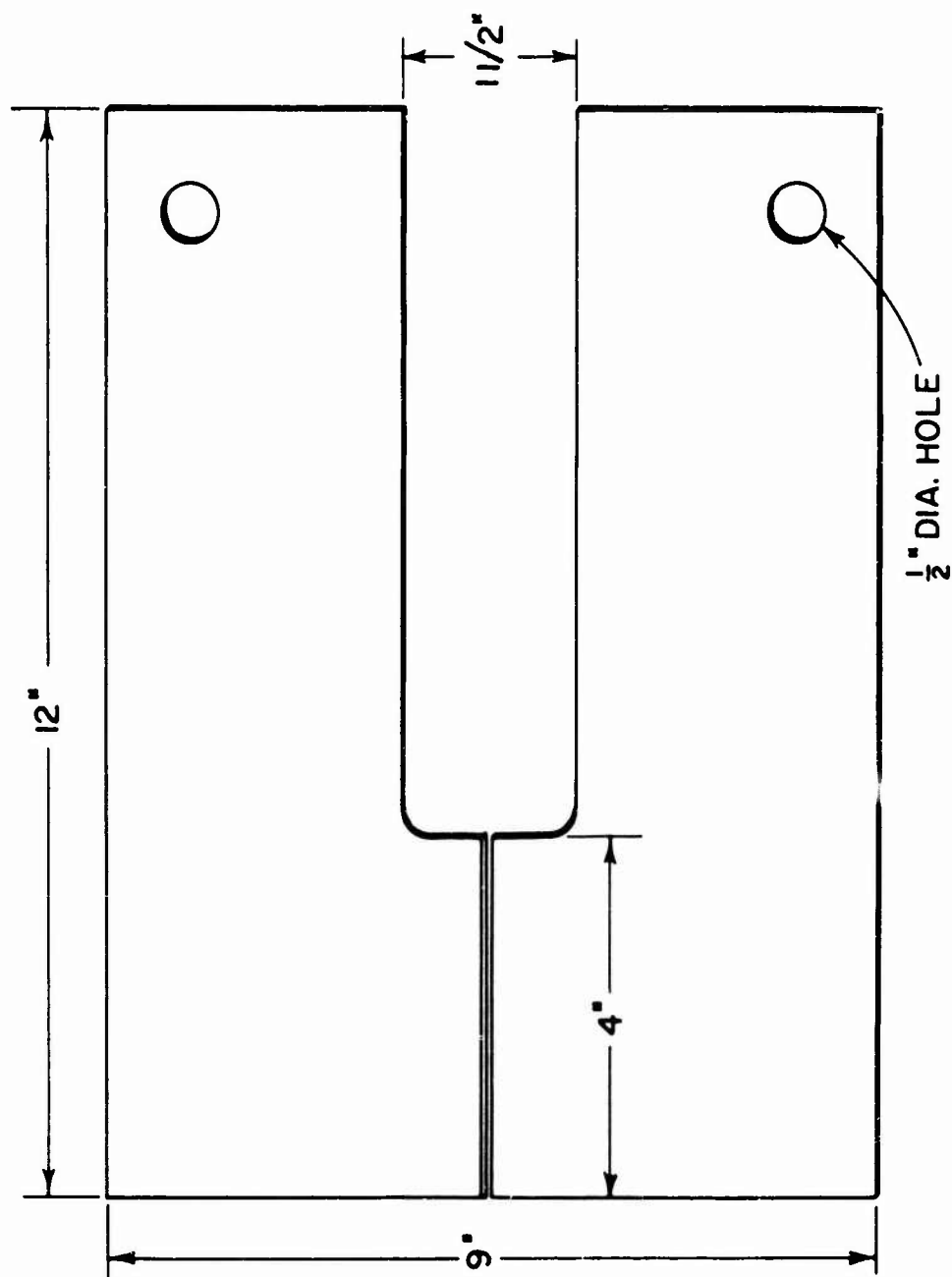


Figure 5. 9 Inch Moment Arm Specimen Design for Horizontal Lever Arms

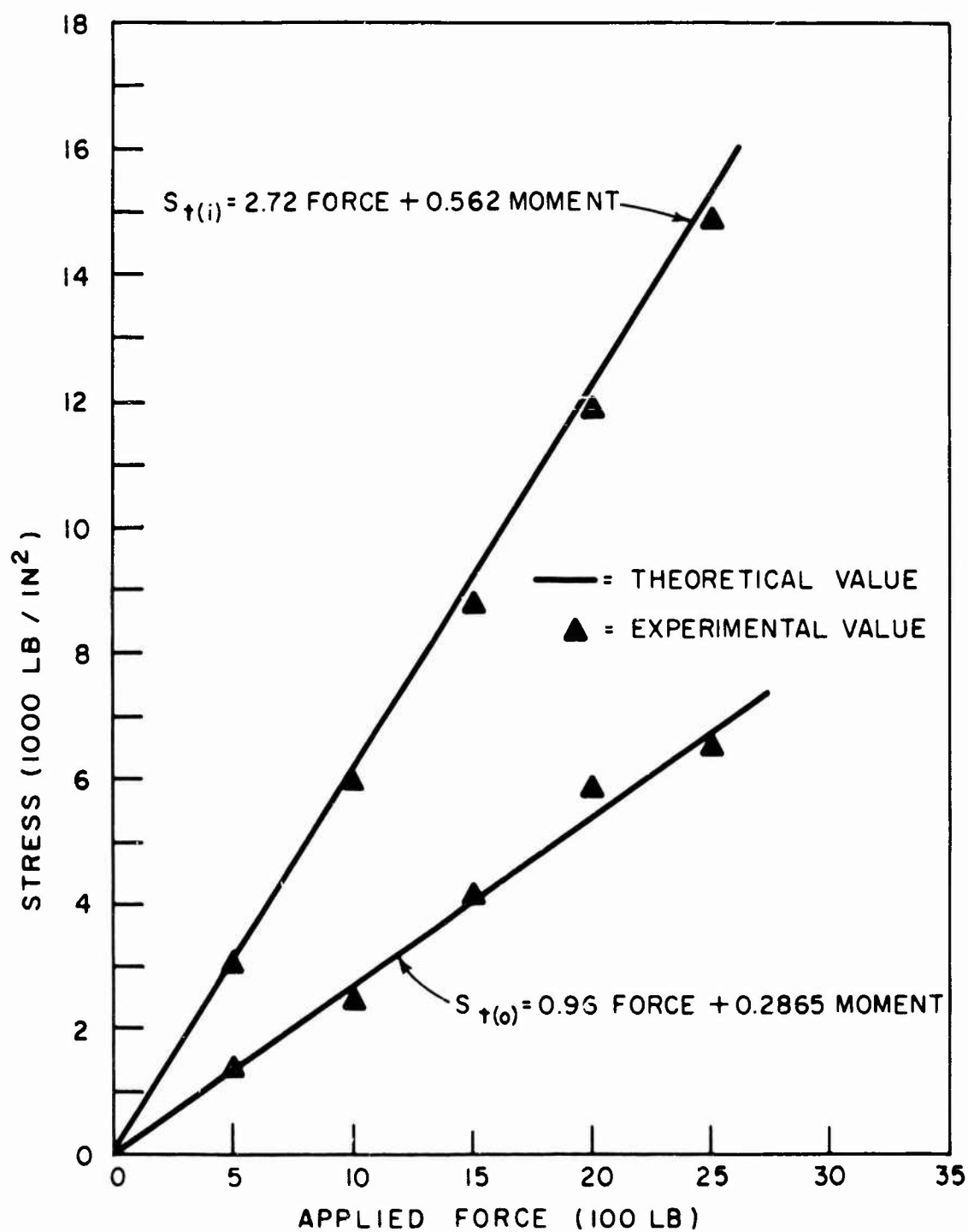


Figure 6. Calculated and Measured Strain Gage Readings for U-bar Calibration

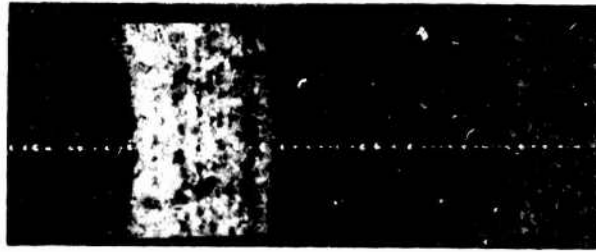


Figure 7. Microstructure of Location Having 1300°F Peak Temperature in HY-80  
 Magnification: 100X                      Nital Etch

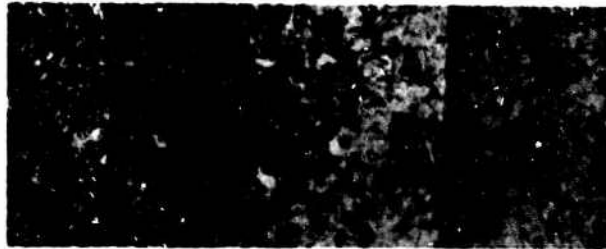


Figure 8. Microstructure of Location Having 1300°F Peak Temperature in HY-80  
 Magnification: 500X

FD 6-17-5

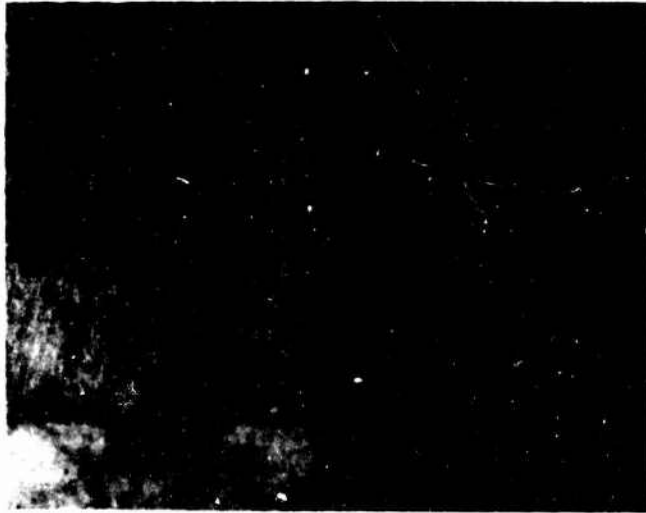


Figure 9. Dendrite Microstructure of Weld Metal in HY-80 Near Fusion  
Boundary

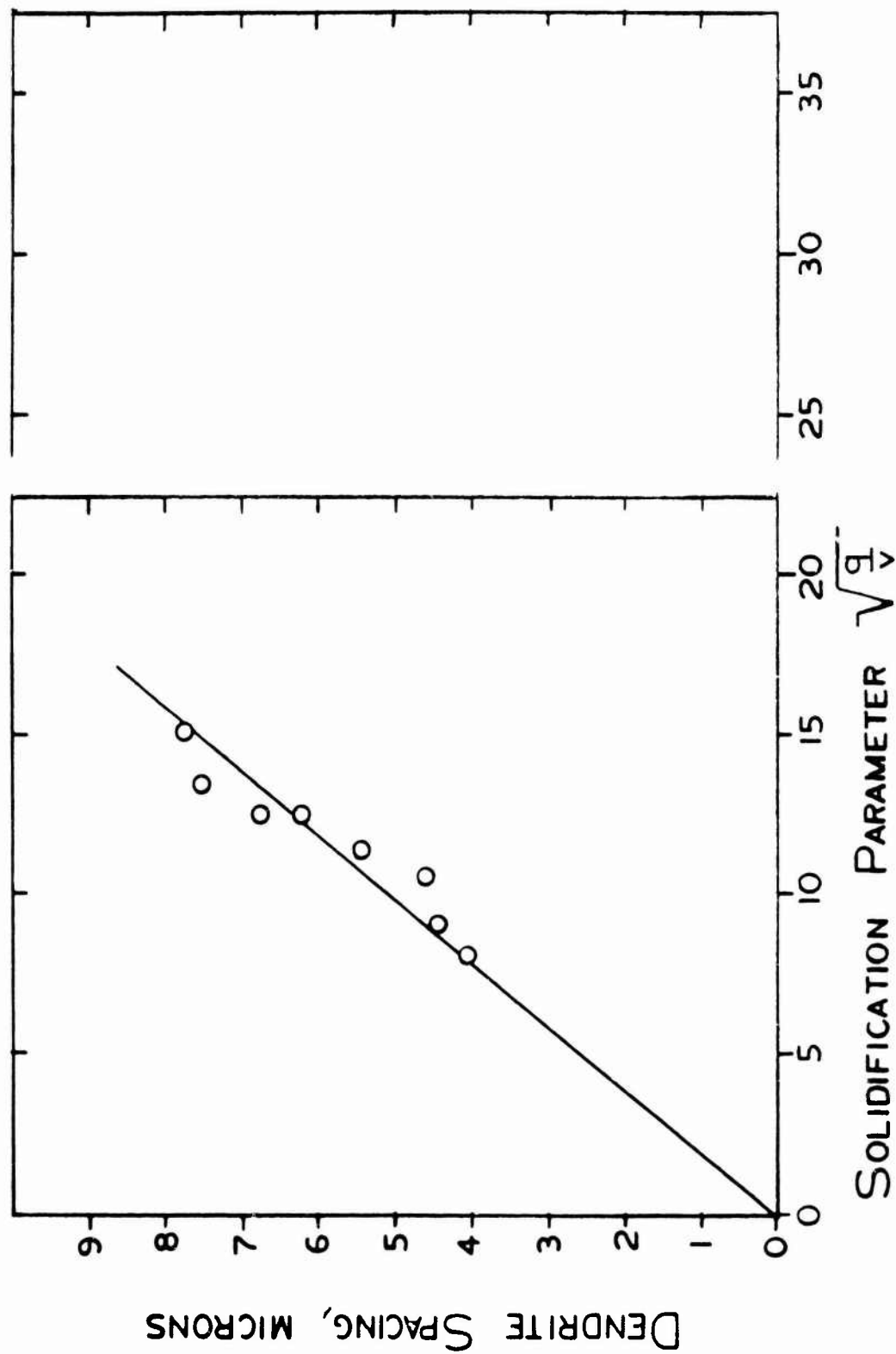


Figure 10. Dendrite Spacing in HY-80 Weld Metal (Near Fusion Boundary)  
as a Function of Arc Energy Input - TIG - No Filler

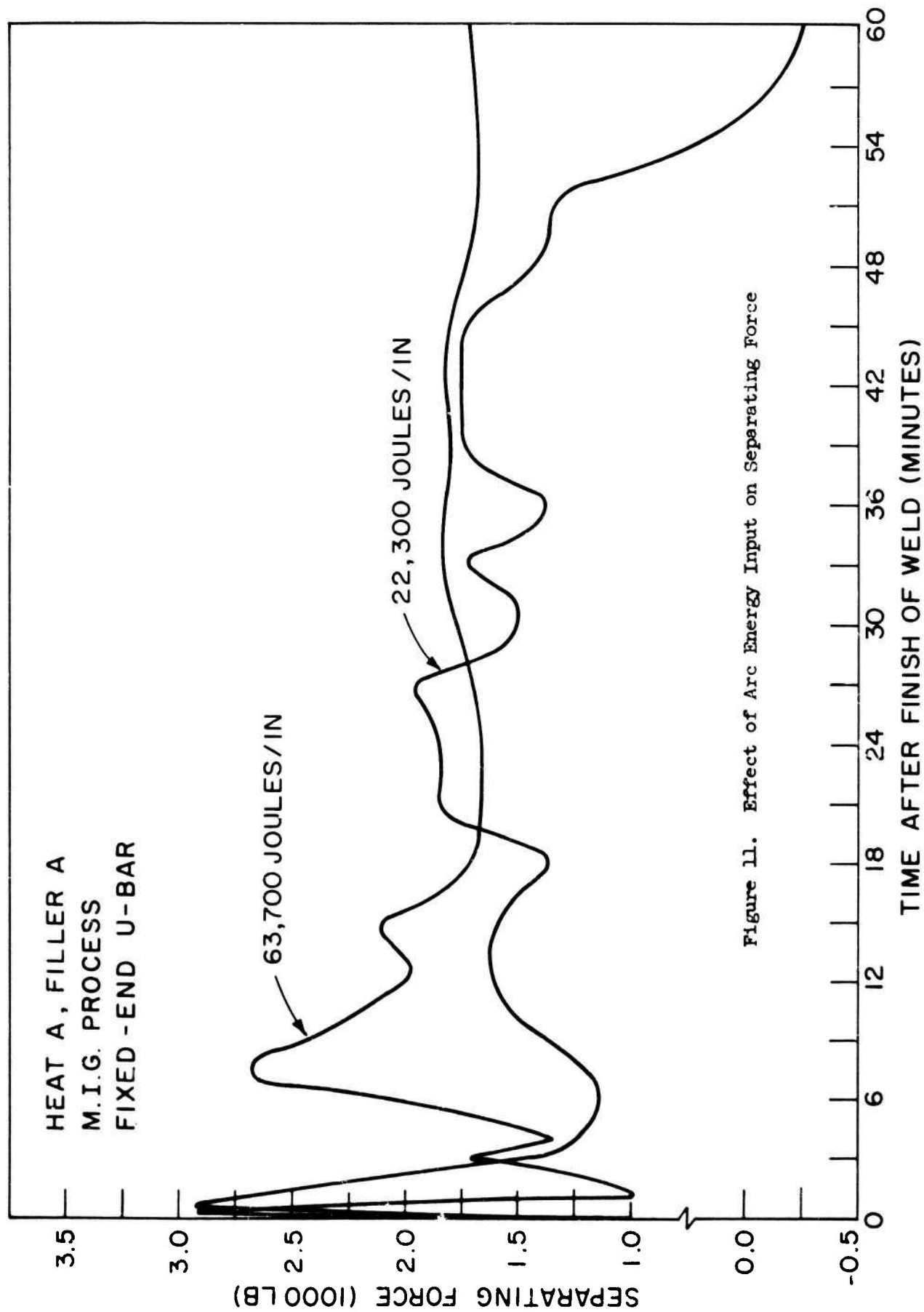


Figure 11. Effect of Arc Energy Input on Separating Force

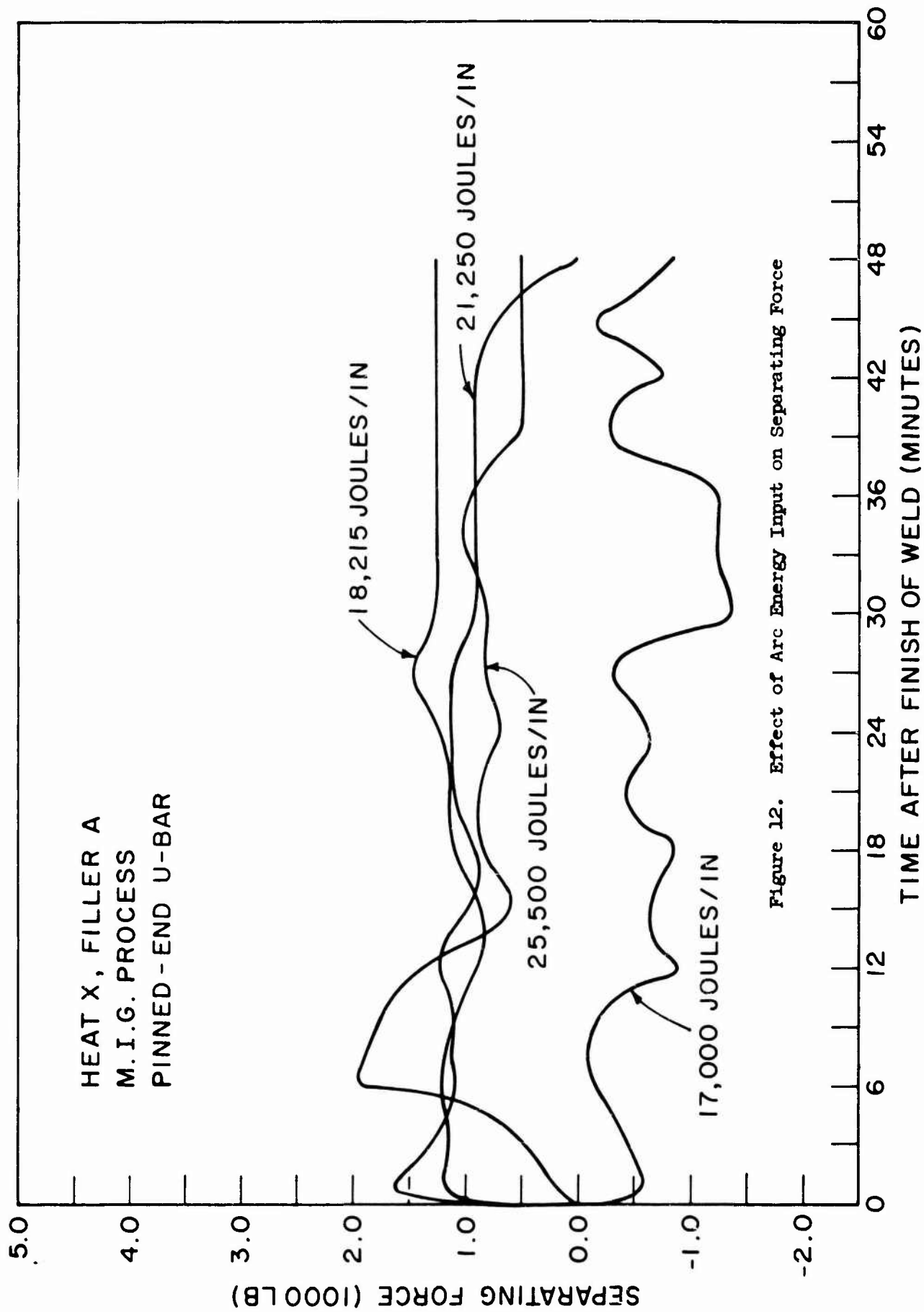


Figure 12. Effect of Arc Energy Input on Separating Force

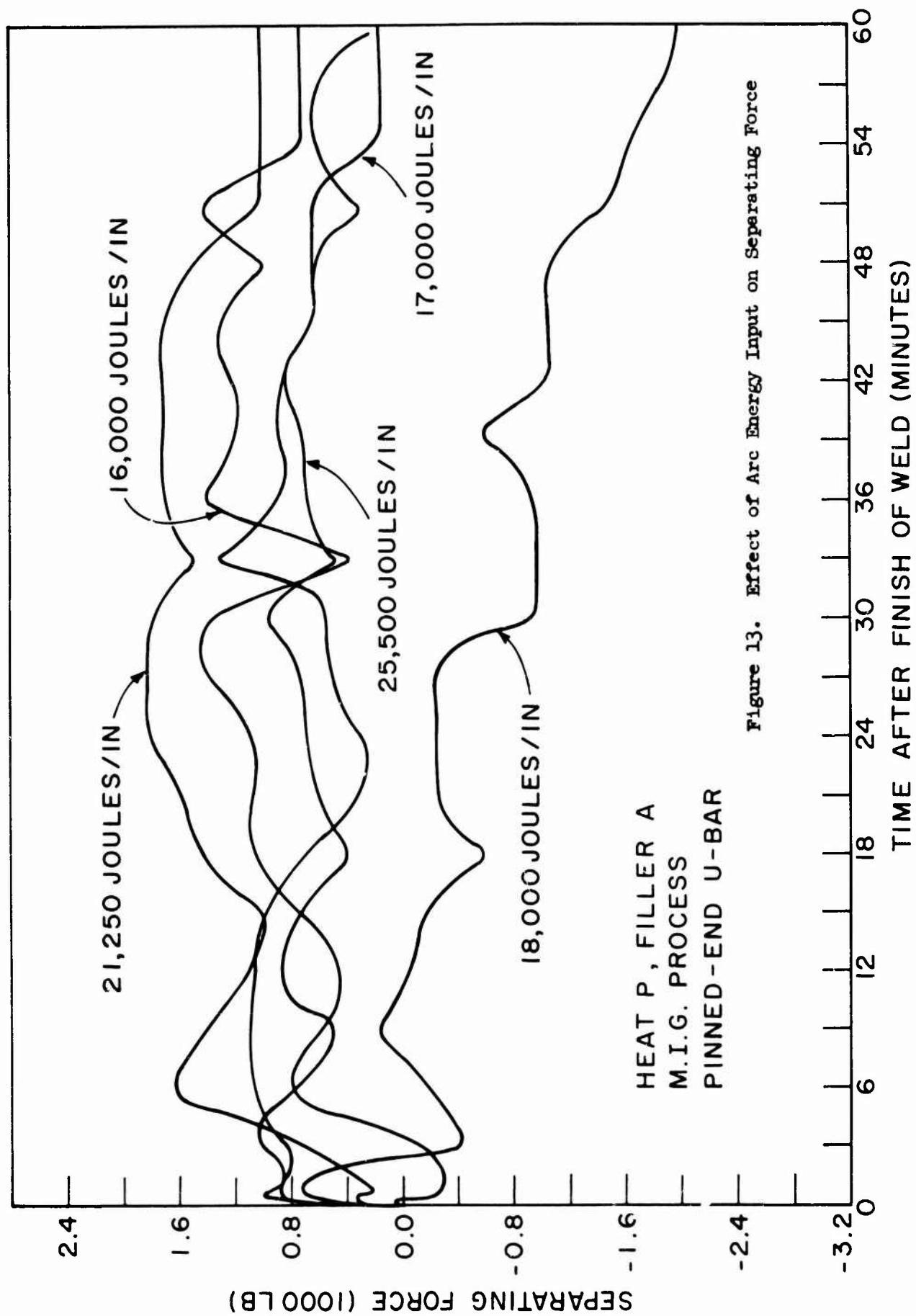


Figure 13. Effect of Arc Energy Input on Separating Force

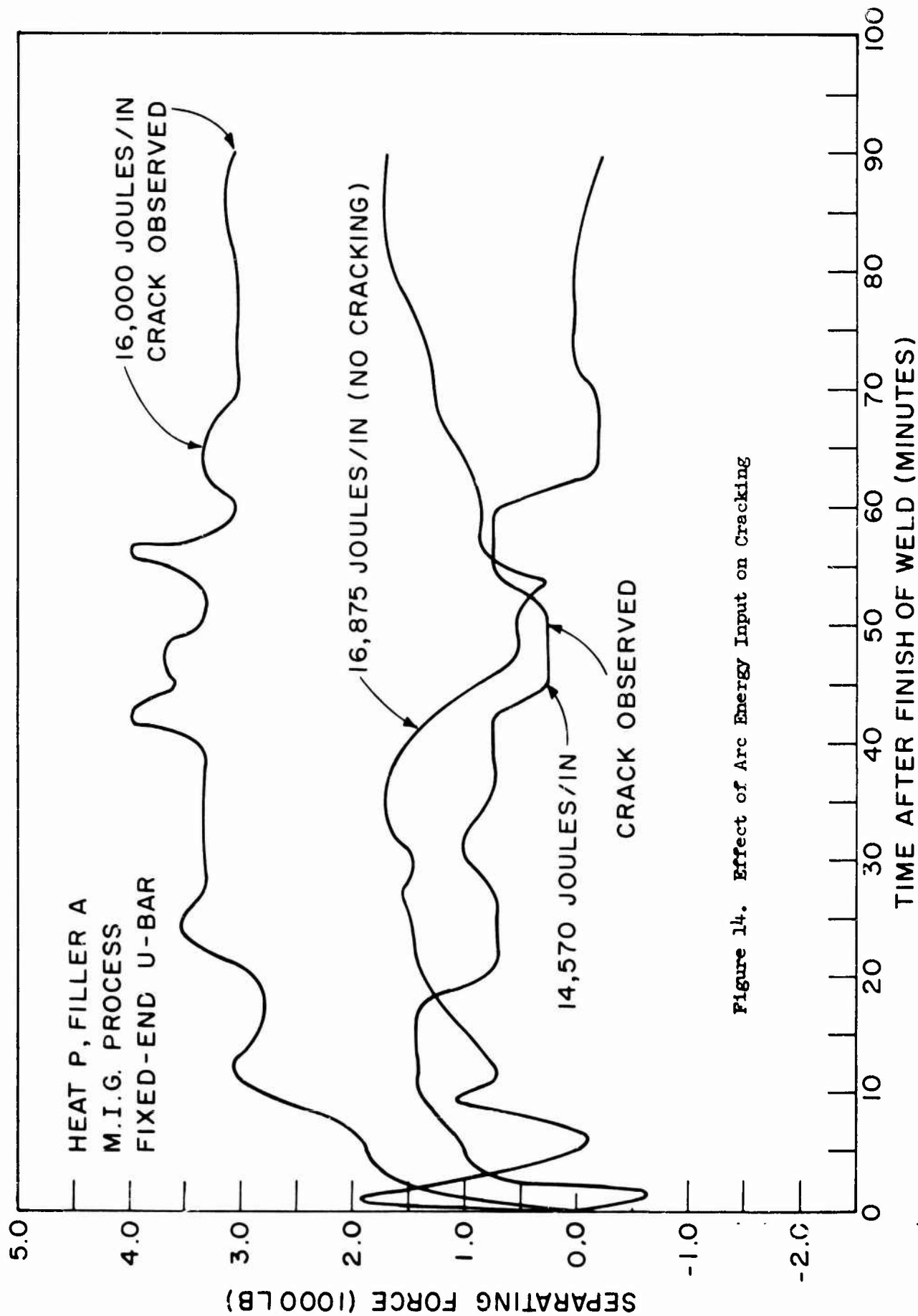


Figure 14. Effect of Arc Energy Input on Cracking

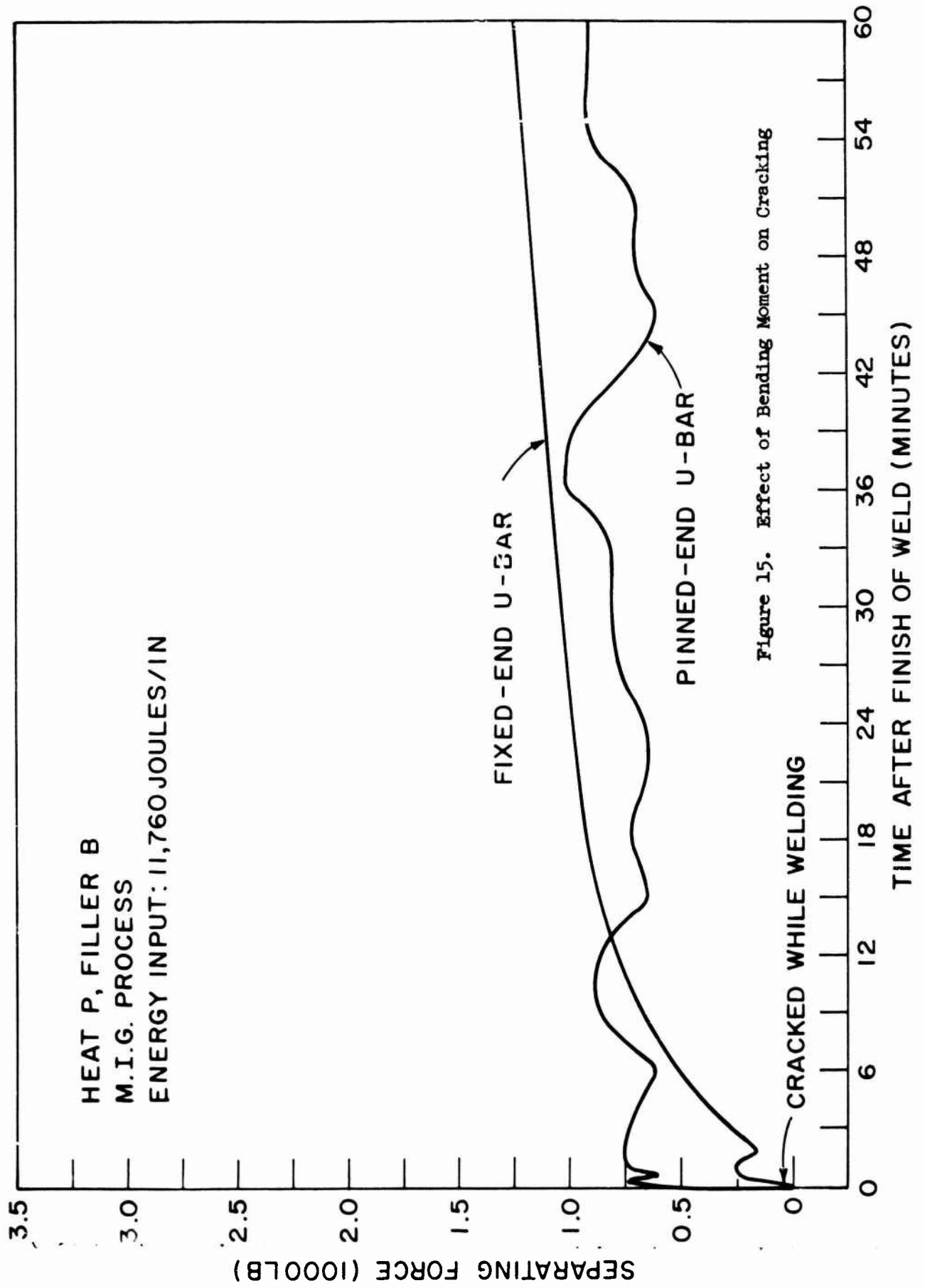


Figure 15. Effect of Bending Moment on Cracking

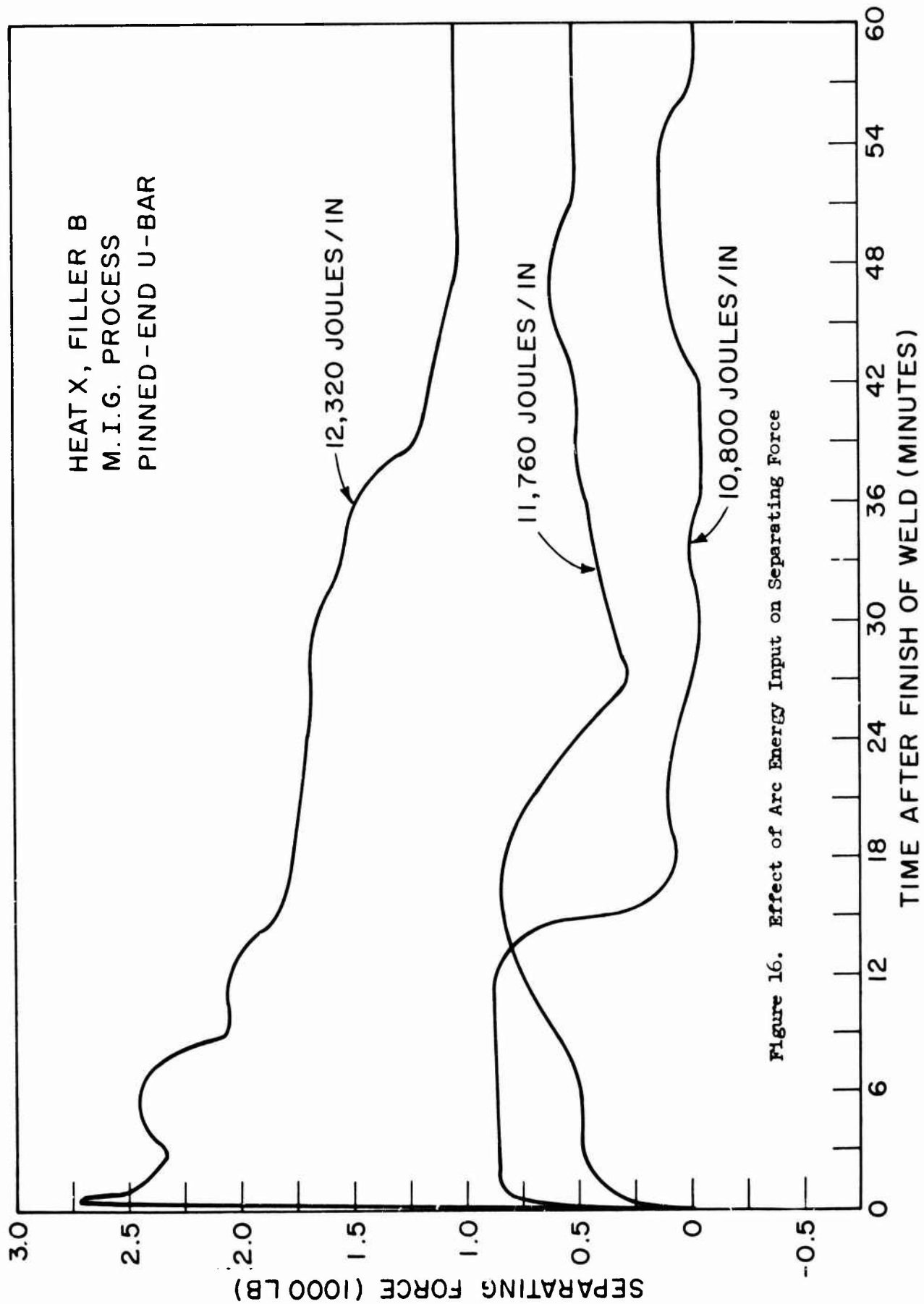


Figure 16. Effect of Arc Energy Input on Separating Force

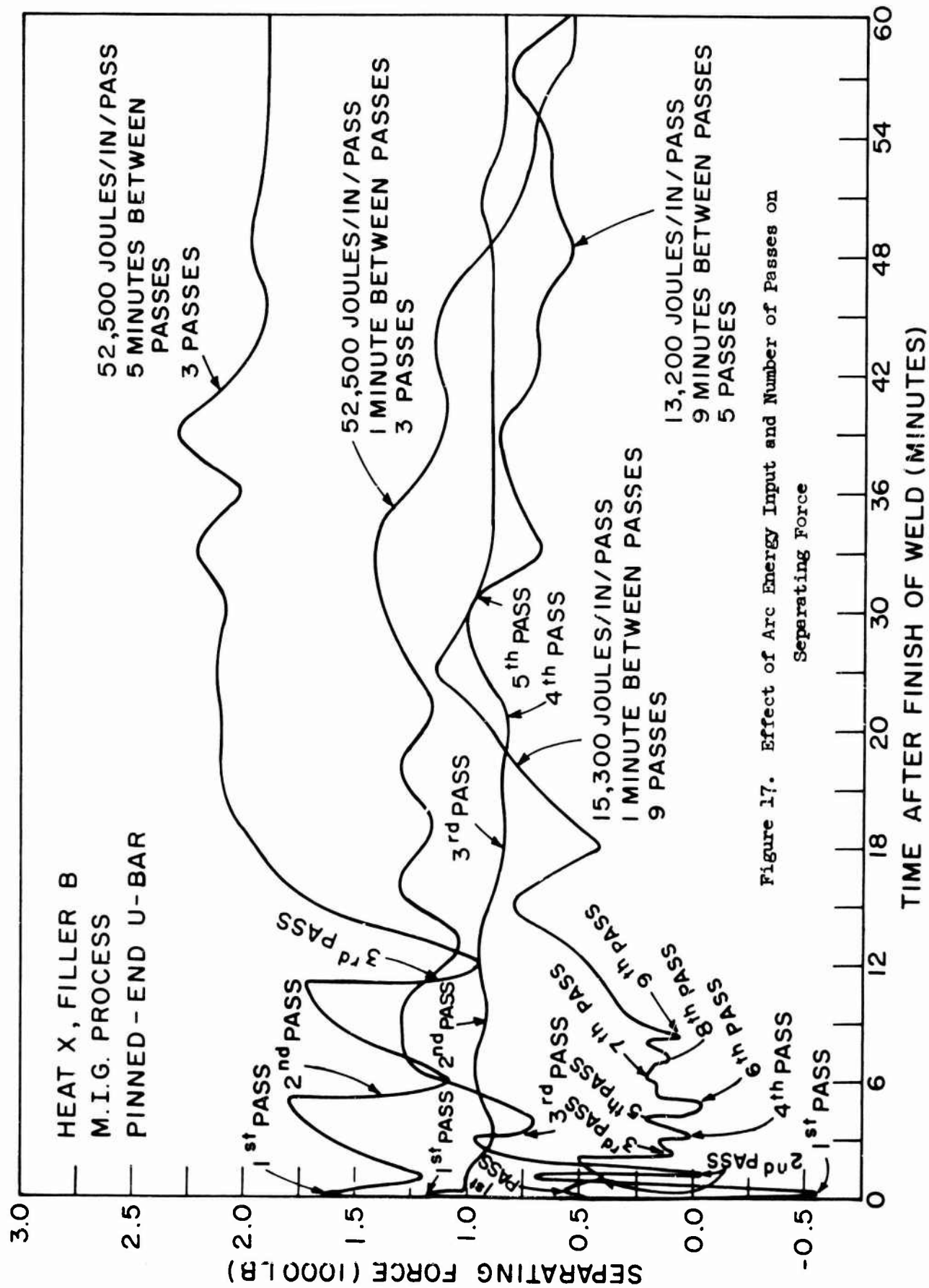


Figure 17. Effect of Arc Energy Input and Number of Passes on Separating Force

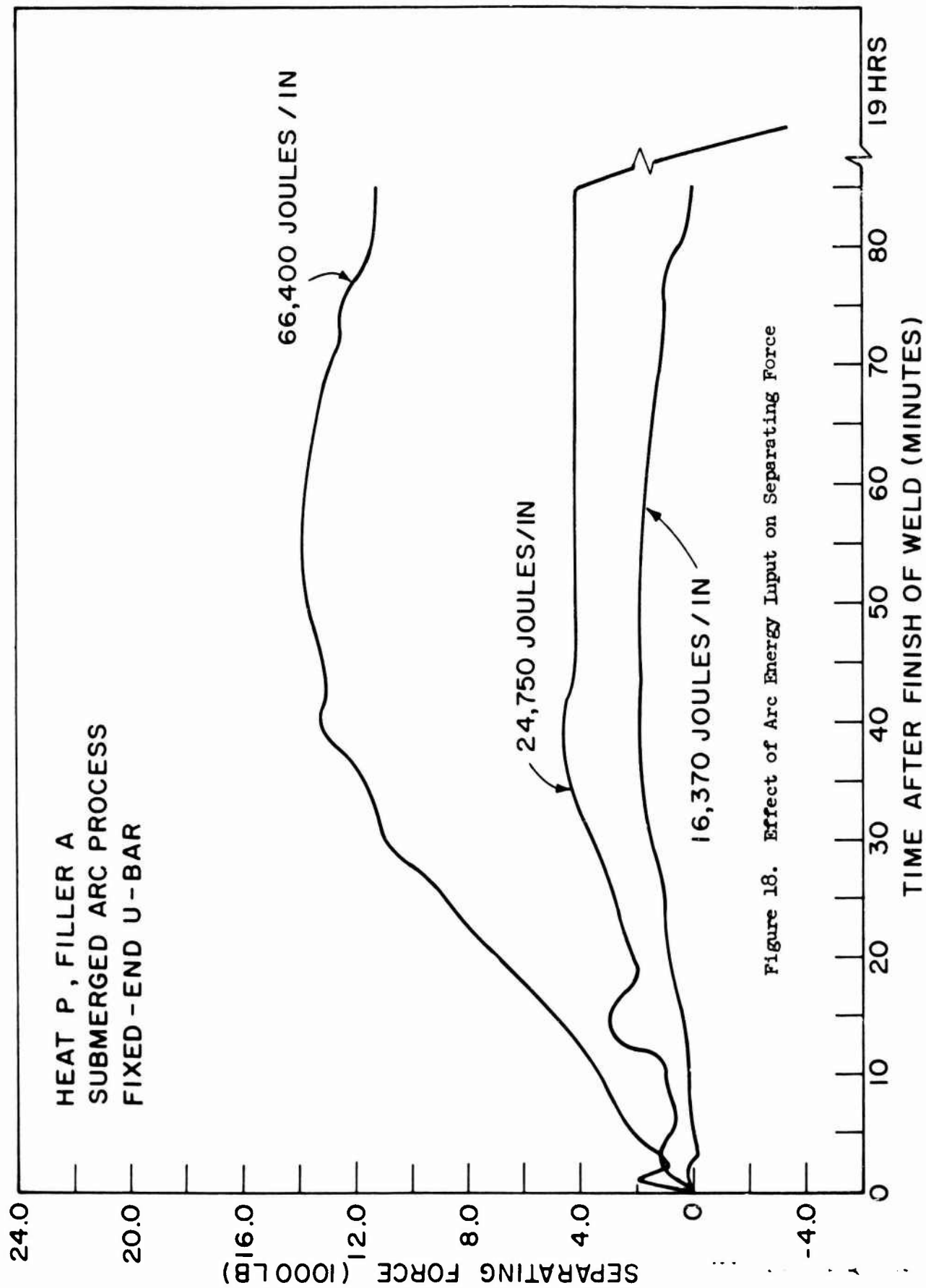


Figure 18. Effect of Arc Energy Input on Separating Force

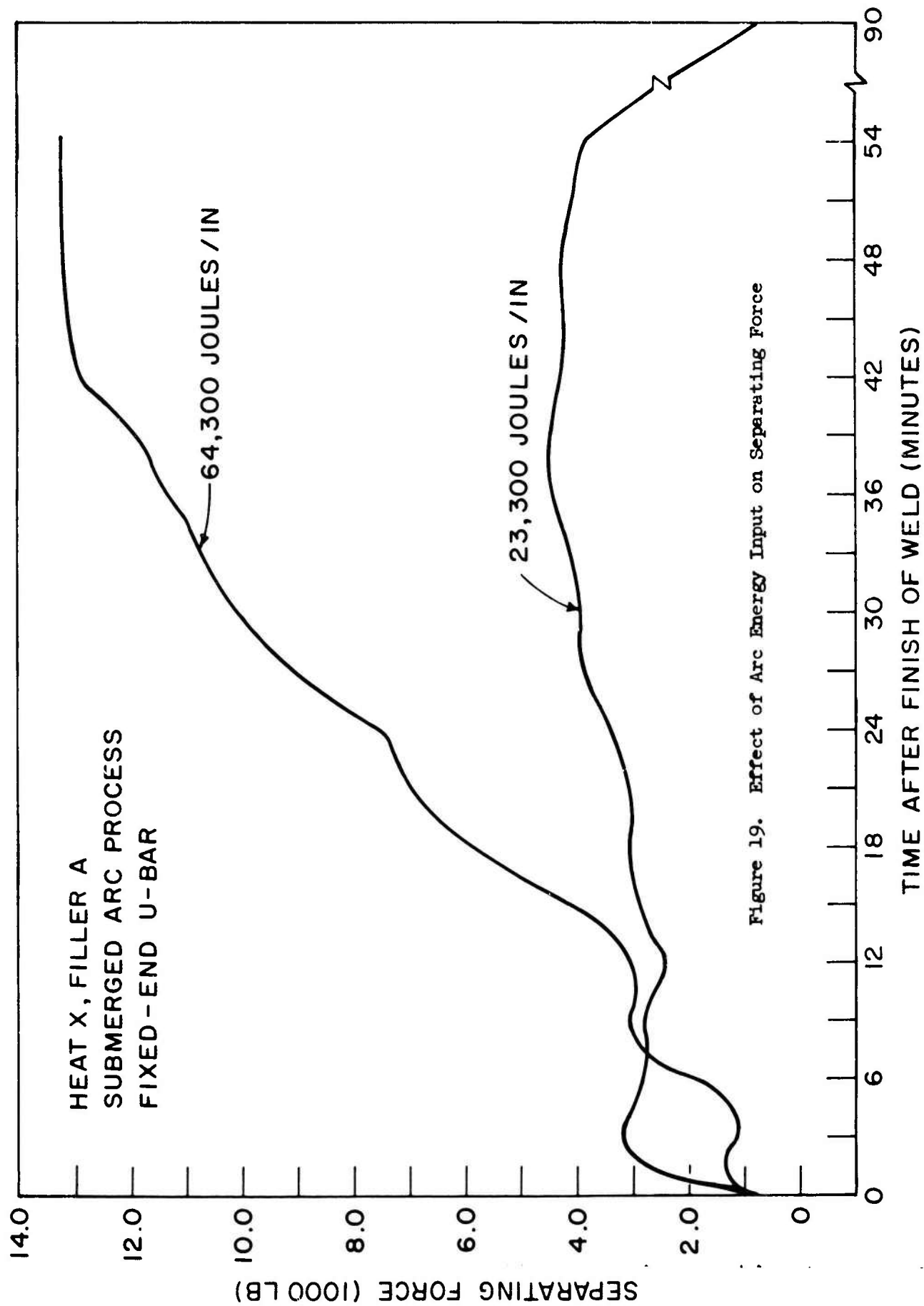


Figure 19. Effect of Arc Energy Input on Separating Force

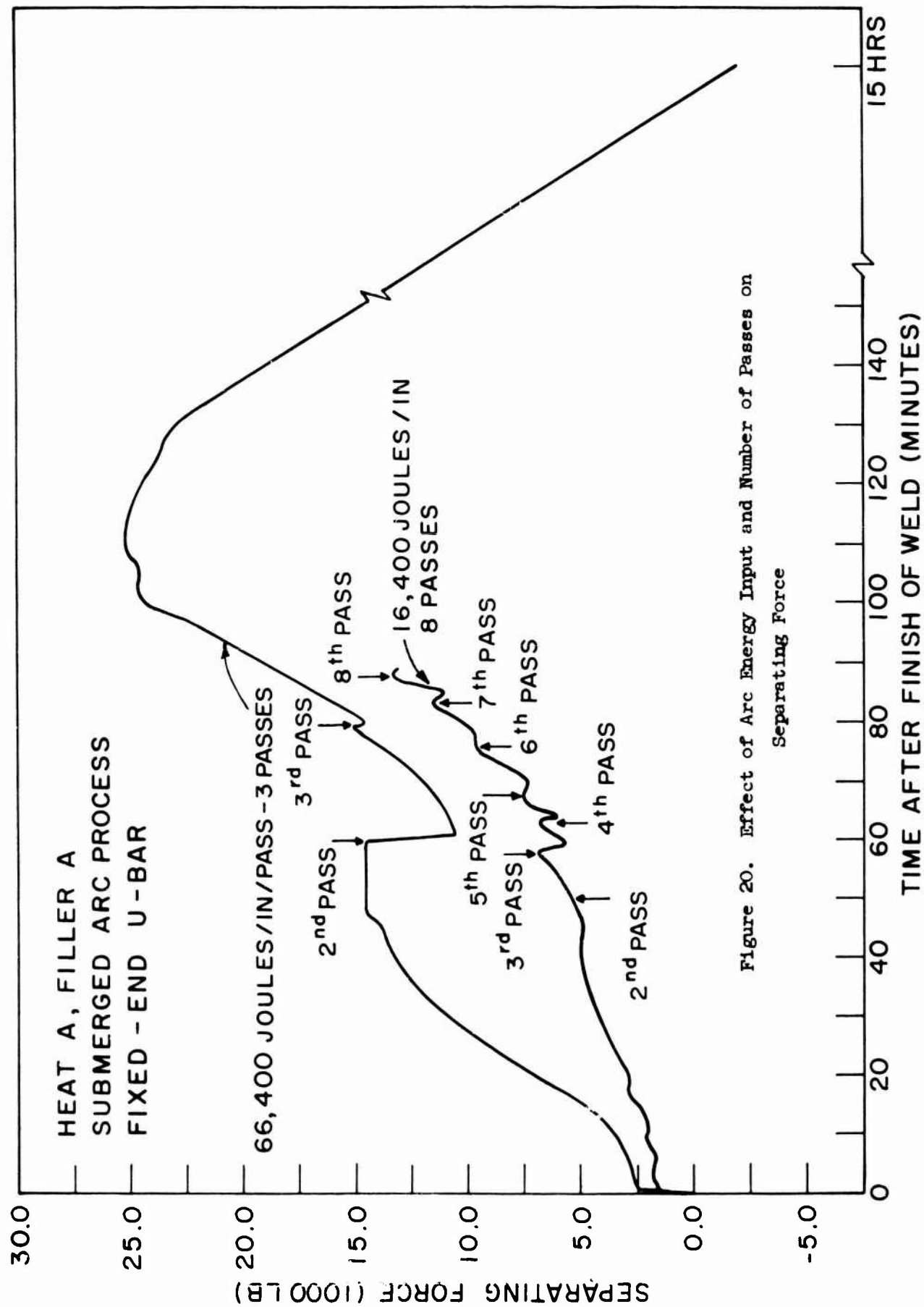
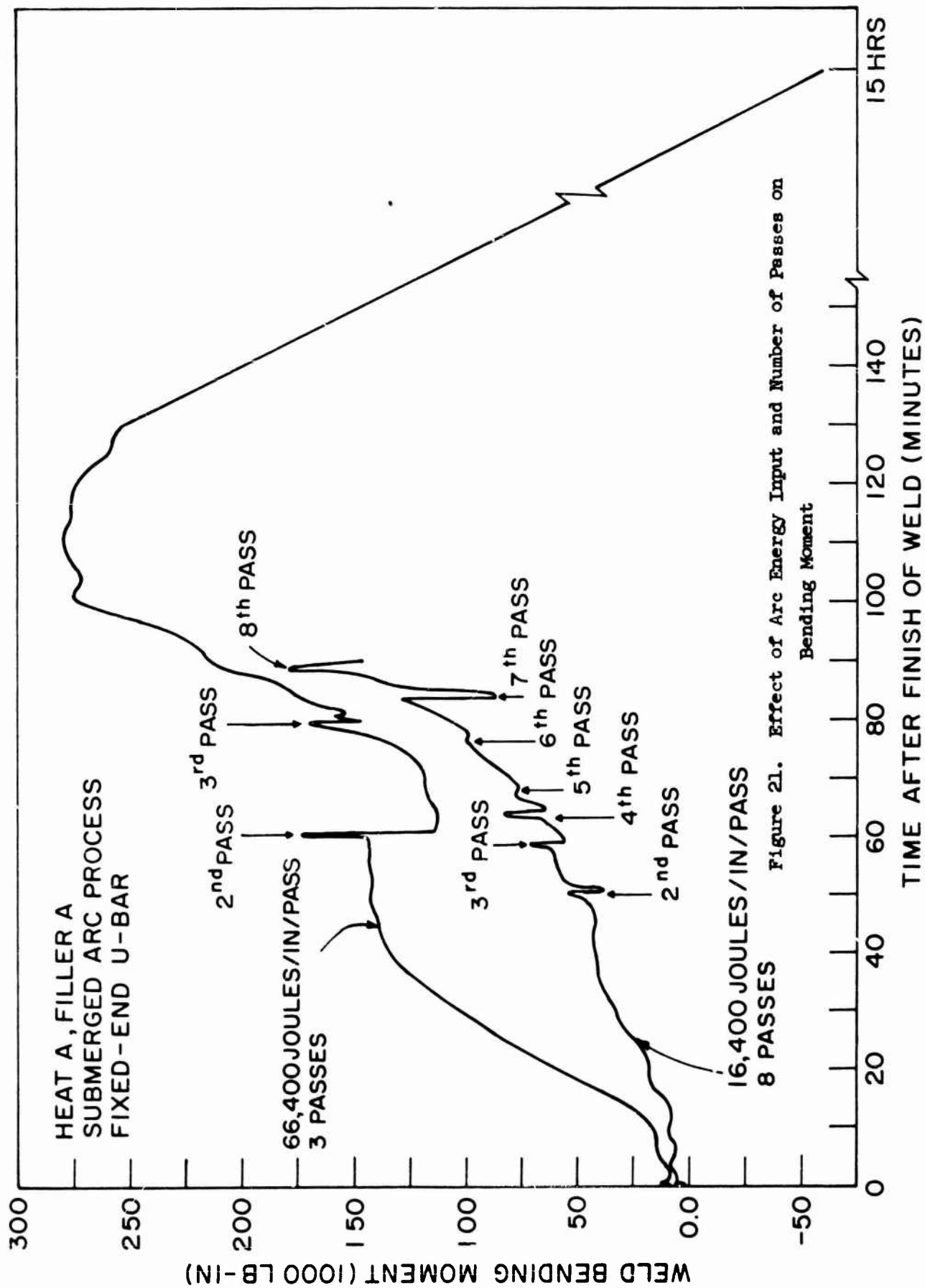


Figure 20. Effect of Arc Energy Input and Number of Passes on Separating Force



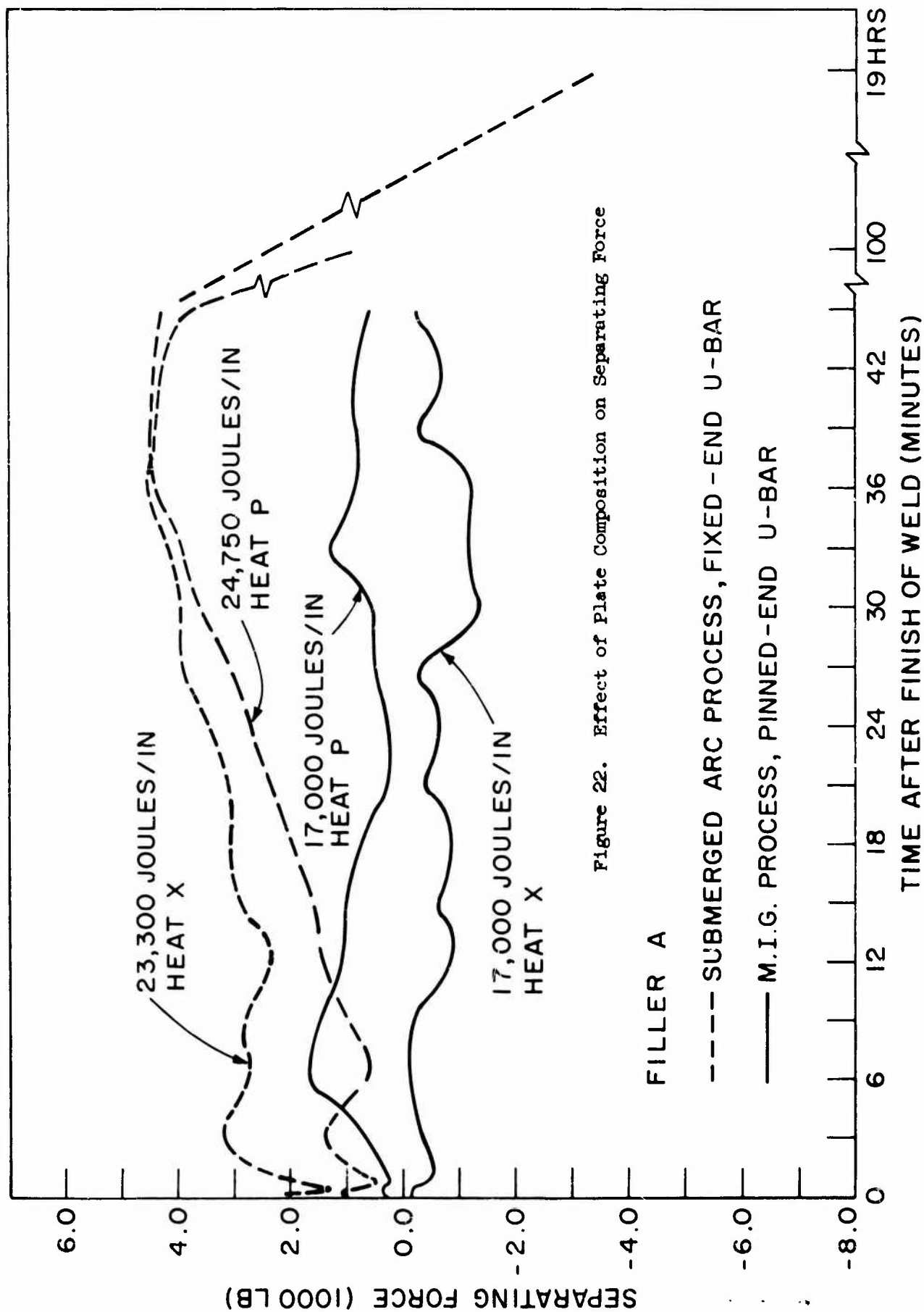


Figure 22. Effect of Plate Composition on Separating Force

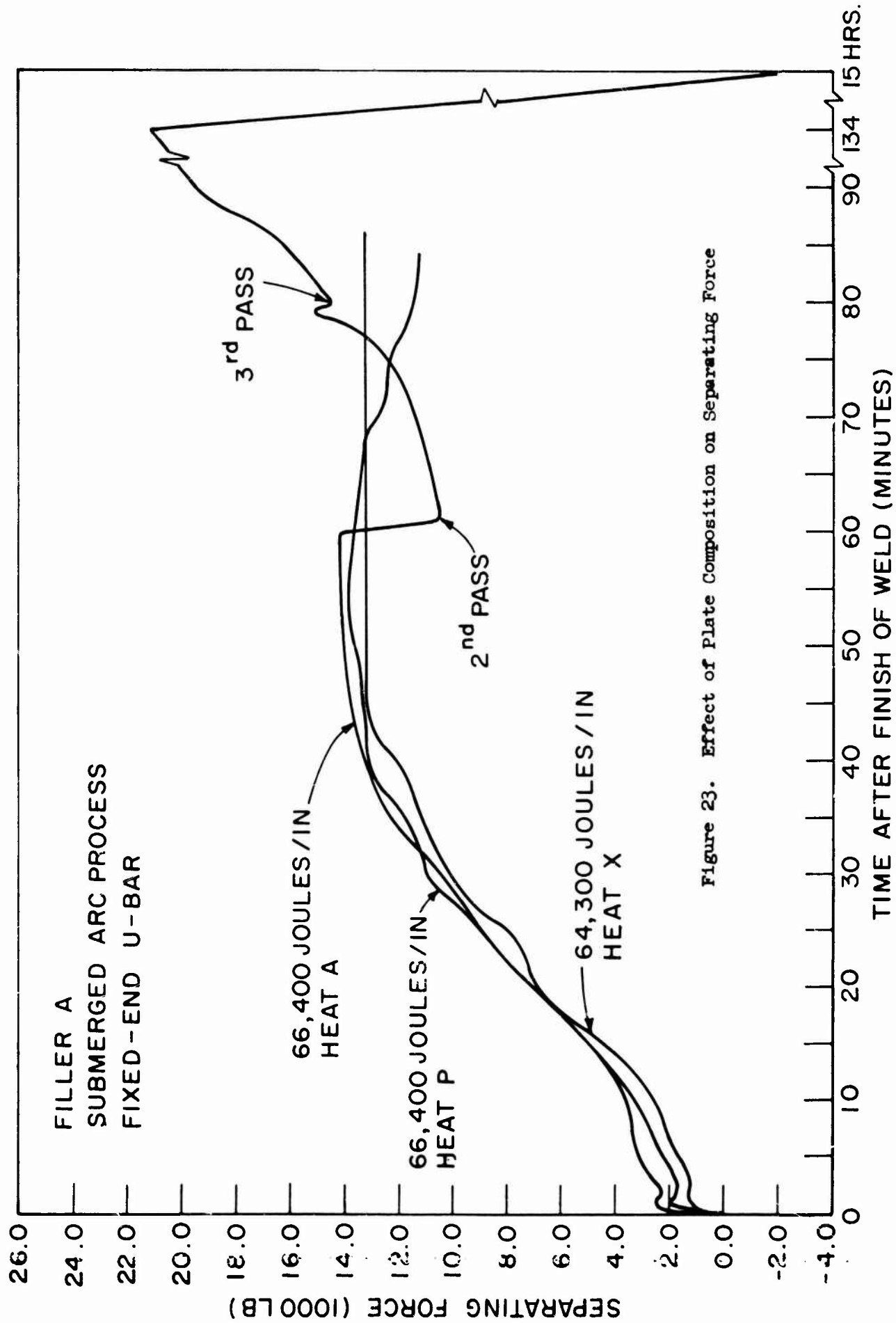


Figure 23. Effect of Plate Composition on Separating Force

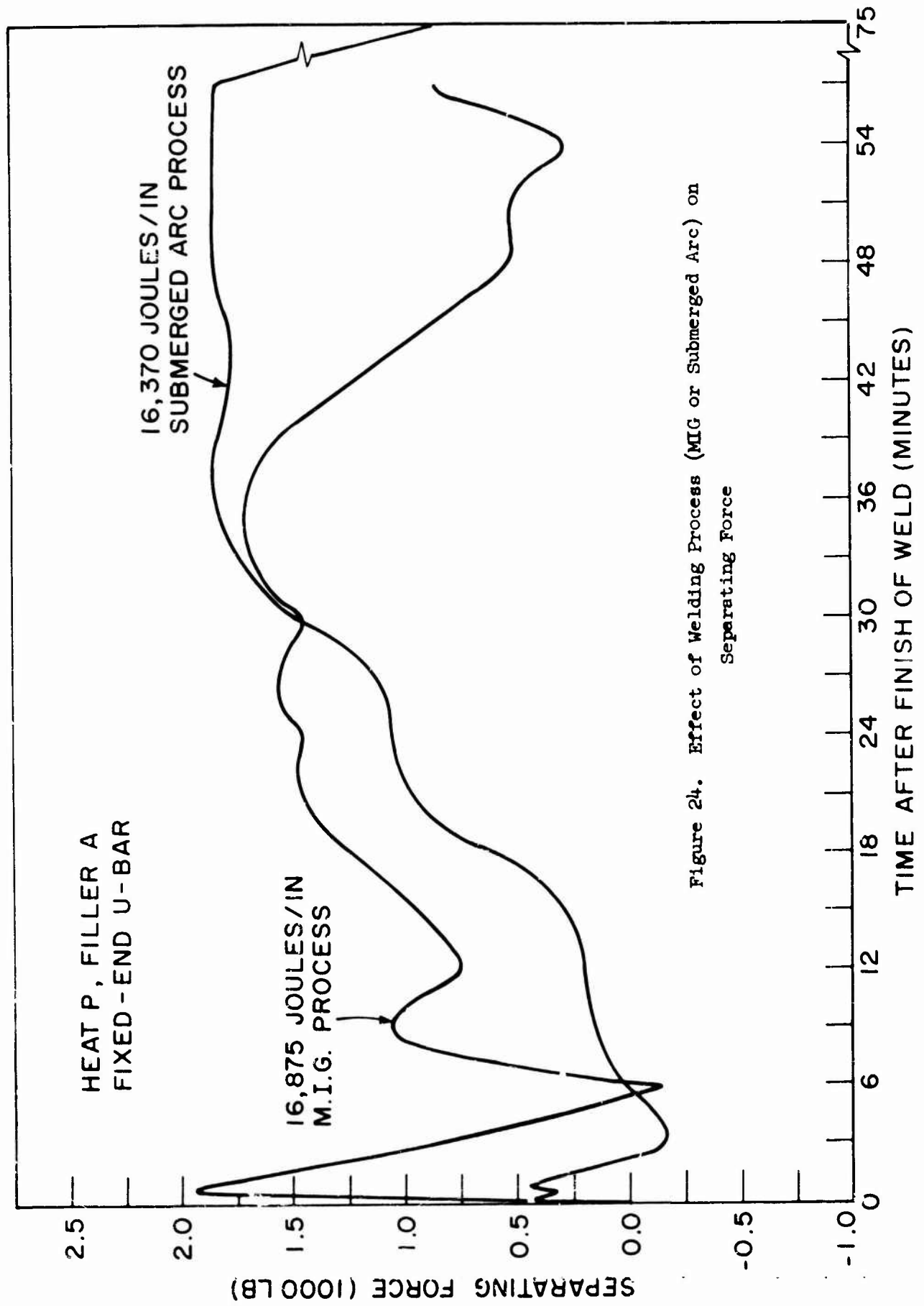


Figure 24. Effect of Welding Process (MIG or Submerged Arc) on Separating Force

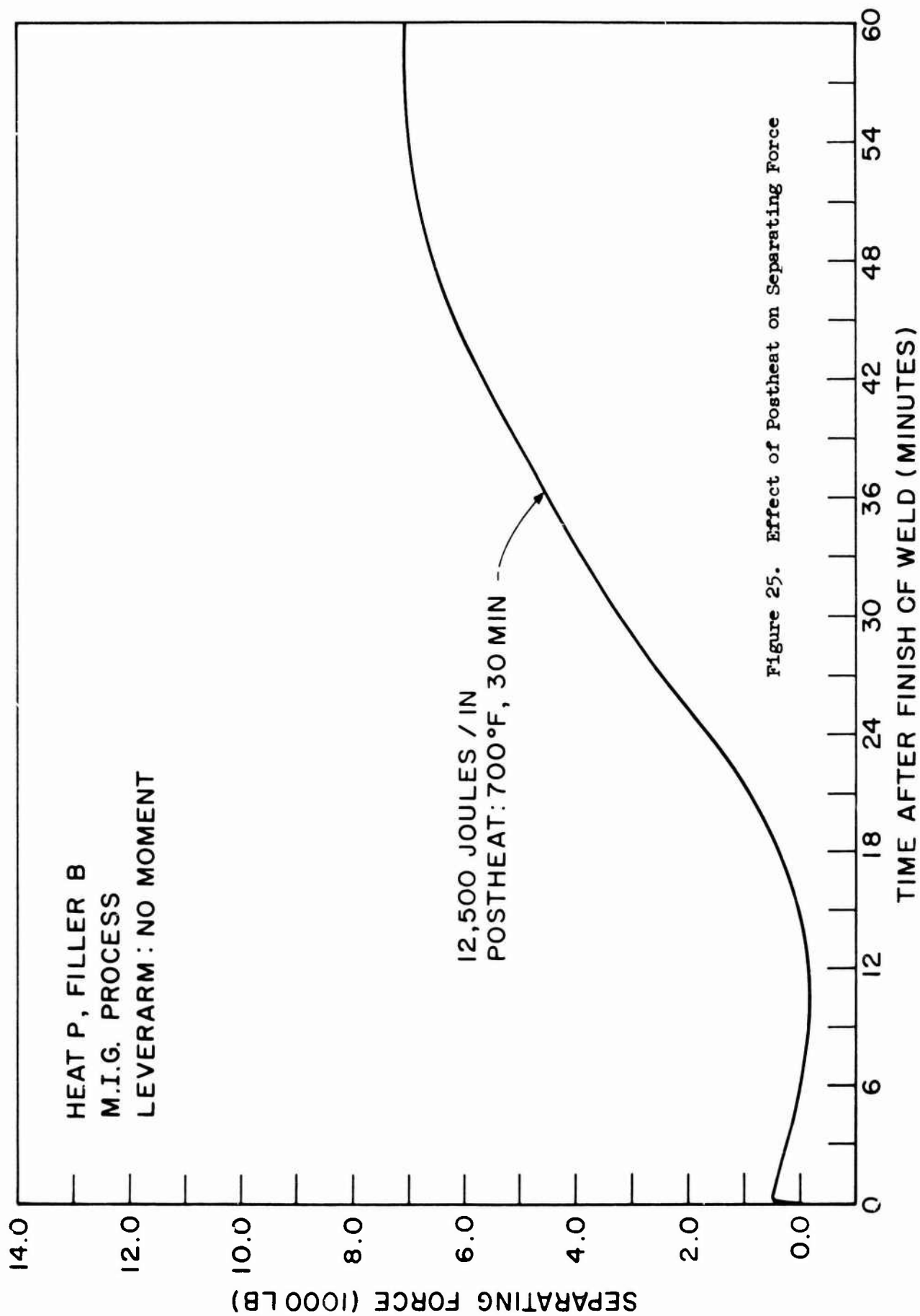


Figure 25. Effect of Postheat on Separating Force